

Past of a quantum particle: Common sense prevails

Berthold-Georg Englert,^{1,2,3,*} Kelvin Horia,^{4,†} Jibo Dai,^{1,‡} Yink Loong Len,^{1,§} and Hui Khoon Ng^{5,1,3,¶}

¹Centre for Quantum Technologies, National University of Singapore, 3 Science Drive 2, Singapore 117543, Singapore

²Department of Physics, National University of Singapore, 2 Science Drive 3, Singapore 117542, Singapore

³MajuLab, CNRS-UNS-NUS-NTU International Joint Unit, UMI 3654, Singapore

⁴Division of Physics and Applied Physics, School of Physical and Mathematical Sciences, Nanyang Technological University, 21 Nanyang Link, Singapore 637371, Singapore

⁵Yale-NUS College, 16 College Avenue West, Singapore 138527, Singapore

(Posted on the arXiv on 12 April 2017; updated on 27 August 2017)

We analyze Vaidman’s three-path interferometer with weak path marking [Phys. Rev. A **87**, 052104 (2013)] and find that common sense yields correct statements about the particle’s path through the interferometer. This disagrees with the original claim that the particles have discontinuous trajectories at odds with common sense. In our analysis, “the particle’s path” has operational meaning as acquired by a path-discriminating measurement. For a quantum-mechanical experimental demonstration of the case, one should perform a single-photon version of the experiment by Danan *et al.* [Phys. Rev. Lett. **111**, 240402 (2013)] with unambiguous path discrimination. We present a detailed proposal for such an experiment.

PACS numbers: 03.65.Ta, 42.50.Dv, 42.50.Xa

I. INTRODUCTION

Vaidman argues that one can meaningfully talk about the past of a quantum particle — specifically: which path it took through an interferometer — by analyzing the faint trace left along the path by weak, almost non-disturbing, measurements within a formalism that uses forward and backward evolving quantum states [1, 2]. He so arrives at conclusions that contradict common sense: The particle can have trajectories that are not continuous. These assertions are confirmed, or so it seems, by an experiment that uses periodic beam deflections at acoustic frequencies to mark the path in an optical three-path interferometer [3]. Various aspects of this matter have been debated [4–35]: whether there is a need for the backward evolving state and the weak values of the two-state formalism, and how to exploit them correctly; whether the experiment can be described by classical optics or by standard quantum-optical methods; whether a consistent-histories description is more appropriate; whether a modified experiment is enlightening; and others. The debate is still going on.

One particular aspect, however, has not yet received the attention it deserves, *viz.* the crucial step of extracting unambiguous which-path information from the faint traces left by an individual particle on its way through the interferometer. This extraction gives operational and quantitative meaning to the otherwise vague concept of “knowledge about the past of the quantum particle.”

We acquire such specific knowledge about the path of a particle just detected by a suitable measurement of the quantum degrees of freedom that are used to mark the path. In this context, what we learn depends much on the question we ask by the chosen measurement, and not all questions are equally relevant. It turns out that common sense prevails if the right question is asked.

Our treatment is entirely within the standard formalism of quantum mechanics and does not rely on the two-state formalism [36, 37] employed by Vaidman. While we do not question the validity of the two-state formalism, we see no particular advantage in using it; the standard formalism offers a transparent way for studying the properties of ensembles that are both pre-selected and post-selected.

We set the stage by reviewing Vaidman’s three-path interferometer in Sec. II, thereby introducing the conventions we use for labeling the four beam splitters, the three paths through the interferometer, and the five checkpoints along the paths. Owing to the high symmetry of the setup, only one common-sense path is available for the particles from the source to the detector.

We then note the description of the pre-selected and post-selected interfering particles in terms of a forward and a backward propagating wave function. Both wave functions are equally crucial in Vaidman’s criterion for establishing where the particle has been at intermediate times. We state this criterion in Vaidman’s words [24] and then recall his narrative of the particles’ history as it follows from his interpretation of the two wave functions and the weak values associated with the three paths. In this narrative the particles propagate along all three paths, which is at odds with the single-path story told by common sense [1].

Section III deals with the weak path marking by which a particle leaves faint traces at the various checkpoints on its way from the source to the detector. We conclude

* cqtebg@nus.edu.sg

† khoria@ntu.edu.sg

‡ Now at Data Storage Institute, A*STAR;

dai_jibo@dsi.a-star.edu.sg

§ yinkloong@quantumlab.org

¶ cqtnhk@nus.edu.sg

that destructive interference suppresses the traces at two checkpoints, which explains why a particle has a discontinuous trajectory in Vaidman's narrative.

Then, in Sec. IV, we examine the faint traces left by the particle just detected. Unambiguous path knowledge — with an operational and quantitative meaning — is available for a small fraction of the particles, and the path is unknown for all others. Upon noting that the probability amplitudes processed by the final beam splitter are incoherent, we present an argument that the particles with unknown path have, in fact, followed the common-sense path; in the limit of ever fainter traces, these are all particles. This conclusion is further supported by an examination of the subensembles of unambiguously known paths or an utterly unknown path and also by the considerations of Sec. V where we re-examine the faint traces by another measurement.

In Sec. VI, we take a close look at the two-path interferometer in Vaidman's three-path setup. We confirm that every particle detected at the exit for destructive interference has a known path, and explain why this is consistent with unknowable paths as the precondition for perfect interference, constructive or destructive. Vaidman's narrative is at odds with common sense for the two-path interferometer, too; in addition, the weak values for the paths have singular imaginary parts.

We propose a single-photon experiment for the two-path interferometer with weak path marking in Sec. VII. An account of the laboratory realization of this proposal will be reported elsewhere [38].

Finally, in Sec. VIII we propose a single-photon version of the three-path interferometer experiment of Ref. [3]. This proposal has not been realized as yet. Once performed, it will demonstrate that common sense does prevail.

II. VAIDMAN'S THREE-PATH INTERFEROMETER

Vaidman's three-path interferometer of Ref. [1] is depicted in Fig. 1 with the labeling conventions of Ref. [3]. The particle (photon or otherwise) is emitted by source S and detected by detector D, which it can reach along either one of the three paths identified by the five checkpoints A, B, C, E, and F. The setup is symmetric because the unitary three-by-three matrices for beam splitters BS1 and BS4 are the same as are the matrices for beam splitters BS2 and BS3 [39],

$$U_1 = U_4 = \frac{1}{\sqrt{3}} \begin{pmatrix} \sqrt{3} & 0 & 0 \\ 0 & -1 & \sqrt{2} \\ 0 & \sqrt{2} & 1 \end{pmatrix},$$

$$U_2 = U_3 = \frac{1}{\sqrt{2}} \begin{pmatrix} 1 & 1 & 0 \\ -1 & 1 & 0 \\ 0 & 0 & \sqrt{2} \end{pmatrix}. \quad (1)$$

They act on three-component columns of probability amplitudes associated with the paths labeled I, II, or III in Fig. 1.

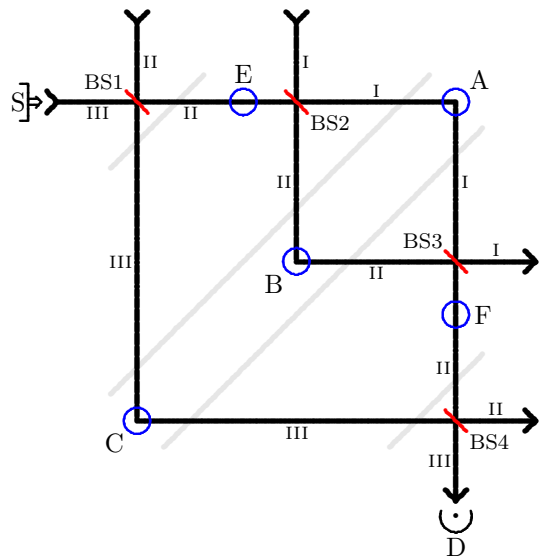


FIG. 1. Vaidman's three-path interferometer of Ref. [1]. The quantum particle is emitted by source S, enters the interferometer at beam splitter BS1, and is detected by detector D after exiting at beam splitter BS4. On the way from S to D, the particle can take the path through checkpoint C, or the paths through the internal Mach-Zehnder loop identified by checkpoints A and B. As a consequence of a weak coupling to the path-marker degrees of freedom, the particle leaves faint traces at these checkpoints, which enable the experimenter to infer the path actually followed. The additional checkpoints at E and F monitor passage into and out of the internal loop. The faint slanted lines connect simultaneous points on the three paths.

For instance, the column $(0 \ 0 \ 1)^\dagger$ stands for the particle emerging from source S and also for the state probed by detector D. With no relative phases introduced in the various links inside the interferometer, the probability that D detects the next particle emitted by S is

$$\left| \begin{pmatrix} 0 \\ 0 \\ 1 \end{pmatrix}^\dagger U_4 U_3 U_2 U_1 \begin{pmatrix} 0 \\ 0 \\ 1 \end{pmatrix} \right|^2 = \frac{1}{9}. \quad (2)$$

Figure 2 gives a more detailed account: The thickness of the blue lines is proportional to the probability of finding the particle there, should we look for it. As a consequence of the symmetry of the setup, the particle has equal chance of being found at checkpoints A, B, or C. We note that the Mach-Zehnder interferometer of the internal loop is balanced, so that the particles do not pass checkpoint F. Accordingly, common sense tells us that all particles detected by D followed the path through checkpoint C and none of them came along EAF or EBF.

This common-sense conclusion is not shared by Vaidman [1]. At the heart of his reasoning is a second state for which the relative probabilities are indicated by the thickness of the red lines. This fictitious state addresses the following question: How would we need to prepare

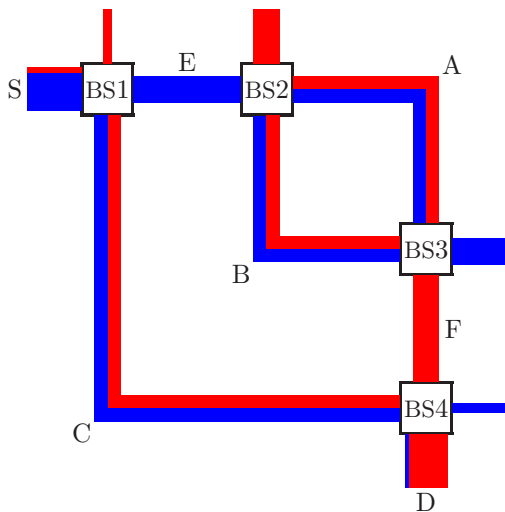


FIG. 2. Probabilities of finding the quantum particle between the source and the detector. The thickness of the blue lines is proportional to the probability of finding the quantum particle there if we look for it. There are equal probabilities of $\frac{1}{3}$ at checkpoints A, B, and C, probability of $\frac{2}{3}$ at E, no probability at F, and the probability of reaching detector D is $\frac{1}{9}$. The red lines refer to the fictitious situation of preparing the quantum particle with non-zero amplitudes at all three entry ports such that it reaches D certainly.

the particle so that it will be surely detected by detector D? Answer: We choose the probability amplitudes

$$\left[\begin{pmatrix} 0 \\ 0 \\ 1 \end{pmatrix}^\dagger U_4 U_3 U_2 U_1 \right]^\dagger = \frac{1}{3} \begin{pmatrix} -\sqrt{6} \\ \sqrt{2} \\ 1 \end{pmatrix}. \quad (3)$$

It is *as if* the particle were injected into the interferometer by the detector and propagating backward in time. There is no mystery here, however. The actual particle emerges from the source and the blue lines in Fig. 2 apply.

Of course, the mathematical formalism offers the flexibility of evaluating the probability amplitudes of Eq. (2) in various ways, depending on which of the matrices in the product $U_4 U_3 U_2 U_1$ act to the right and which act to the left. For each such split, we can find the so-called weak values of the projectors onto the three paths, as illustrated by

$$\left(\frac{1}{3}\right)^{-1} \begin{pmatrix} 0 \\ 0 \\ 1 \end{pmatrix}^\dagger U_4 U_3 \begin{pmatrix} 1 \\ 0 \\ 0 \end{pmatrix} \begin{pmatrix} 1 \\ 0 \\ 0 \end{pmatrix}^\dagger U_2 U_1 \begin{pmatrix} 0 \\ 0 \\ 1 \end{pmatrix} = -1 \quad (4)$$

for path I in the symmetric split. The normalizing prefactor divides by the amplitude that is squared in Eq. (2). By definition, then, the weak values for the three paths have unit sum for each split.

The three weak values for all five splits are reported in Table I. We observe that all three weak values have

TABLE I. The weak values of the projectors on the three paths for different ways of splitting the product $U_4 U_3 U_2 U_1$ into operators acting to the right and to the left. The projectors are inserted at the split, indicated by the vertical line $|$. All U s act to the right in the first row, all act to the left in the last row.

split	weak values		
	I	II	III
$ U_4 U_3 U_2 U_1$	0	0	1
$U_4 U_3 U_2 U_1$	0	0	1
$U_4 U_3 U_2 U_1$	-1	1	1
$U_4 U_3 U_2 U_1$	0	0	1
$U_4 U_3 U_2 U_1 $	0	0	1

unit magnitude for the symmetric split of the third row, which refers to projecting on the paths at checkpoints A, B, and C. For all other splits, the weak values for paths I and II vanish.

Consistent with this observation, we have coexisting blue and red lines in Fig. 2, of equal thickness even, on the path along checkpoint C and also inside the internal loop. In Vaidman's view, the particle could only have been in these regions where we have both the blue and the red probabilities [24]:

$$\text{The particle was present in paths of the interferometer in which there is an overlap of the forward and backward evolving wave functions.} \quad (5)$$

In his narrative of the particle's history on the way from the source to the detector, then, the particle was inside the internal loop at intermediate times, but it did not pass checkpoint E (no red probability) nor checkpoint F (no blue probability): The particle was inside the loop but it did not enter or leave. At a certain instant, the particle was at checkpoints A *and* B *and* C simultaneously [40] (and could have left a weak trace at all three checkpoints).

Yet, we surely find the one particle traversing the interferometer in one place only whenever we look for it. Nobody is looking, however. It is impossible to reconcile this narrative with common sense.

One could shrug and leave it at that. As outrageous as they may be, we cannot test statements about the particle's whereabouts unless we observe it on its way from the source to the detector. This observation has to be gentle on the particle in order to not disturb the delicate balance of the interferometer. Something of this kind is accomplished by the weak path marking in the optical experiment reported by Danan *et al.* in Ref. [3]. And, yes, the data show equally strong traces from checkpoints A, B, and C but no traces from checkpoints E and F; see Fig. 3, where we reproduce the power spectrum of Figs. 2(b) and 3 in [3].

Yes, these data are consistent with Vaidman's narrative, but does the experiment really demonstrate the case? No, it doesn't, for at least two reasons. First,

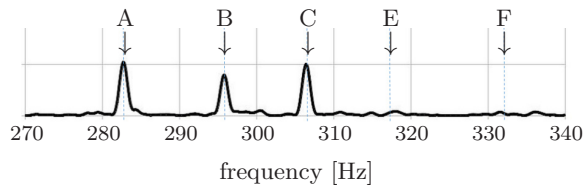


FIG. 3. Data collected in the experiment by Danan *et al.* [3]. In this optical version of Vaidman’s three-path interferometer, light propagates through the interferometer in a horizontal plane. Path information is encoded by slightly deflecting the light beams out of this plane. This is achieved by mirrors (not drawn in Fig. 1) at the checkpoints that oscillate about a horizontal axis with a small amplitude. The resulting upward or downward displacement at the detector (~ 600 nm) is quite small compared with the transverse coherence length of the light (~ 1.2 mm) in order to ensure the weakness of the path marking. The detector registers separately the light intensities above and below the horizontal plane, and the squared Fourier transform of their difference is the reported power spectrum, reproduced here from Figs. 2(b) and 3 in [3]. The five mirrors at the five checkpoints oscillate with different frequencies between 280 Hz and 335 Hz, so that the five well-separated peaks in the power spectrum can be associated with individual mirrors. The peaks for checkpoints A, B, and C are of about equal height and much higher than those for checkpoints E and F, which are buried in the noise.

the experiment is performed with classical light intensities, and one does not need quantum mechanics for a comparison with theoretical predictions; Maxwell’s electrodynamics is quite sufficient. Although one could invoke that, for such linear-optics circumstances, there is a one-to-one correspondence between light intensities and photon probabilities [41], it remains true that the experiment by Danan *et al.* does not make any information available about individual photons.

Second, the data are perfectly consistent with an alternative story: Each photon of a small fraction leaves a discernible trace at checkpoint A *or* at B *or* at C, while most photons leave no trace at all. This interpretation of the data, which is as natural as that offered in [3] if not more so, does not support Vaidman’s criterion (5). (As discussed in Sec. III, the peaks for checkpoints E and F are suppressed by destructive interference.)

On the basis of the data reported by Danan *et al.*, one cannot tell whether Vaidman’s narrative or the alternative story is correct. A single-photon version of the experiment is needed to decide the matter. Zhou *et al.* [32] do send single photons through the three-path interferometer, but their detection method is unable to extract all the available path information, and as such is little better than the original experiment in resolving the narrative. We present a proposal for a single-photon experiment that achieves full path-information extraction in Sec. VIII.

Such a single-photon experiment allows for a meaningful statement about the path taken by the photon just detected. The data of the classical-light experiment are

good enough for ensemble averages (expectation values). Whether an individual photon leaves a trace at A, at B, or at C, however, can only be inferred in a single-photon experiment. Our analysis concerns this single-photon situation, and the weak values of Table I play no role in it. We predict that the data of an experiment with single photons will speak against Vaidman’s narrative and in favor of the alternative story.

III. WEAK PATH MARKING

The oscillating-mirror method of imprinting a path mark on the light in the experiment of Danan *et al.* [3], see the caption to Fig. 3, does not lend itself to extraction of path knowledge about an individual photon, should one execute the experiment in a single-photon fashion. Statements of the kind “the particle (= photon) is inside the internal loop after passing checkpoint E and before reaching checkpoint F” take for granted that the photon is sufficiently localized — having a longitudinal extension of 3 cm, say, roughly one-tenth of the distance between beam splitters BS2 and BS3 (an example of Vaidman’s “localized wave packet” [1]). Then, the photon takes ~ 0.1 ns to pass a point on its trajectory. The mirrors, which have oscillation periods of several milliseconds, are standing still for lapses of time so short. None of the frequencies of the mirror oscillations is imprinted on the photon. An individual photon is simply deflected up or down a bit, either by the mirror at checkpoint C or jointly by the mirrors at E, A or B, and F.

We cannot infer the path taken from the observed deflection, as we cannot tell which mirror(s) deflected the photon [42]. Therefore, we do not examine the experiment of Danan *et al.* [3] in further detail, and rather exploit entanglement of a more immediately useful kind for the path marking and the extraction of path information.

For the path marking, we use weak interactions at the checkpoints, described by unitary operators A , B , C , E , and F that differ slightly from the identity operator and act on certain quantum degrees of freedom other than the path degree of the interferometer. These marker degrees of freedom are initially not correlated with the particle’s path degree of freedom, and we write ρ for the statistical operator of the initial path-marker state.

Then, the very small probability ϵ that the next particle reaches checkpoint F is

$$\epsilon = \text{tr}\{T_F \rho T_F^\dagger\} = \langle T_F^\dagger T_F \rangle, \quad (6)$$

where the trace is over the path-marker degrees of freedom and

$$T_F = \begin{pmatrix} 0 \\ 1 \\ 0 \end{pmatrix}^\dagger U_3 \begin{pmatrix} A & 0 & 0 \\ 0 & B & 0 \\ 0 & 0 & C \end{pmatrix} U_2 \begin{pmatrix} 1 & 0 & 0 \\ 0 & E & 0 \\ 0 & 0 & 1 \end{pmatrix} U_1 \begin{pmatrix} 0 \\ 0 \\ 1 \end{pmatrix}$$

$$= \frac{1}{\sqrt{6}}(B - A)E \quad (7)$$

so that

$$\epsilon = \frac{1}{6} \langle E^\dagger (B - A)^\dagger (B - A) E \rangle. \quad (8)$$

We have $0 < \epsilon \ll 1$ under the weak path-marking circumstances of interest, when the particle leaves but a faint trace of its path through the interferometer.

The unnormalized final state of the path marker, conditioned on the particle detection by D, is $T_{\text{fin}} \rho T_{\text{fin}}^\dagger$ with

$$\begin{aligned} T_{\text{fin}} &= \begin{pmatrix} 0 \\ 0 \\ 1 \end{pmatrix}^\dagger U_4 \begin{pmatrix} 1 & 0 & 0 \\ 0 & F & 0 \\ 0 & 0 & 1 \end{pmatrix} U_3 \begin{pmatrix} A & 0 & 0 \\ 0 & B & 0 \\ 0 & 0 & C \end{pmatrix} U_2 \\ &\times \begin{pmatrix} 1 & 0 & 0 \\ 0 & E & 0 \\ 0 & 0 & 1 \end{pmatrix} U_1 \begin{pmatrix} 0 \\ 0 \\ 1 \end{pmatrix} = \frac{1}{3} [C + F(B - A)E] \end{aligned} \quad (9)$$

where the coefficients +1, +1, and -1 for C , FBE , and FAE , respectively, are reminiscent of the weak values in Table I but do not have the weak-value meaning. The probability of detecting the particle is

$$\begin{aligned} \text{tr} \{ T_{\text{fin}} \rho T_{\text{fin}}^\dagger \} &= \langle T_{\text{fin}}^\dagger T_{\text{fin}} \rangle \\ &= \frac{1}{9} \langle [C + F(B - A)E]^\dagger [C + F(B - A)E] \rangle, \end{aligned} \quad (10)$$

and the normalized final state of the path marker is

$$\begin{aligned} \rho_{\text{fin}} &= \frac{T_{\text{fin}} \rho T_{\text{fin}}^\dagger}{\langle T_{\text{fin}}^\dagger T_{\text{fin}} \rangle} \\ &= \frac{[C + F(B - A)E] \rho [C + F(B - A)E]^\dagger}{\langle [C + F(B - A)E]^\dagger [C + F(B - A)E] \rangle}. \end{aligned} \quad (11)$$

Since we want to investigate the faint traces left at individual checkpoints, we shall now take for granted that each checkpoint has its own path-marker degree of freedom and that there are no initial correlations between the marker degrees of freedom [43]. Accordingly, A , B , C , E , and F commute with one another and ρ factorizes,

$$\rho = \rho_A \rho_B \rho_C \rho_E \rho_F. \quad (12)$$

Then we have

$$\epsilon = \frac{1}{6} \langle (B - A)^\dagger (B - A) \rangle = \frac{1}{3} - \frac{1}{3} \text{Re}(\langle A \rangle^* \langle B \rangle) \quad (13)$$

and

$$\langle T_{\text{fin}}^\dagger T_{\text{fin}} \rangle = \frac{1 + 6\epsilon}{9} - \frac{2}{9} \text{Re}(\langle (A) - \langle B \rangle \rangle \langle C \rangle^* \langle E \rangle \langle F \rangle) \quad (14)$$

where $\langle X \rangle = \text{tr}_X \{ X \rho_X \}$ for $X = A, B, C, E, F$. We recover $\epsilon = 0$ and $\langle T_{\text{fin}}^\dagger T_{\text{fin}} \rangle = \frac{1}{9}$ for $A = B = 1$, as we should.

The final statistical operator for checkpoint E is obtained by tracing ρ_{fin} over the other checkpoints, with the outcome

$$\begin{aligned} \rho_{\text{E,fin}} &= \frac{1}{9 \langle T_{\text{fin}}^\dagger T_{\text{fin}} \rangle} \left[\rho_E + 6\epsilon E \rho_E E^\dagger \right. \\ &\quad \left. - 2 \text{Re} \left(E \rho_E (\langle A \rangle - \langle B \rangle) \langle C \rangle^* \langle F \rangle \right) \right], \end{aligned} \quad (15)$$

where $\text{Re}(X) = \frac{1}{2}(X + X^\dagger)$ for operator X , and there is an analogous expression for $\rho_{\text{F,fin}}$. The final statistical operator for checkpoint C is

$$\begin{aligned} \rho_{\text{C,fin}} &= \frac{1}{9 \langle T_{\text{fin}}^\dagger T_{\text{fin}} \rangle} \left[C \rho_C C^\dagger + 6\epsilon \rho_C \right. \\ &\quad \left. - 2 \text{Re} \left(\rho_C C^\dagger (\langle A \rangle - \langle B \rangle) \langle E \rangle \langle F \rangle \right) \right]. \end{aligned} \quad (16)$$

We note that 6ϵ multiplies the initial state ρ_C here whereas this factor multiplies the transformed $E \rho_E E^\dagger$ in $\rho_{\text{E,fin}}$.

The symmetry of the interferometer should be affected minimally by the weak measurement. In particular, we do not want to unbalance the internal Mach-Zehnder loop more than is unavoidable. Therefore, we require $\langle A \rangle = \langle B \rangle$, with their values determined by Eq. (13),

$$\langle A \rangle = \langle B \rangle = \sqrt{1 - 3\epsilon} \quad (17)$$

and so arrive at

$$\langle T_{\text{fin}}^\dagger T_{\text{fin}} \rangle = \frac{1 + 6\epsilon}{9} \quad (18)$$

as well as

$$\rho_{\text{E,fin}} = \frac{\rho_E + 6\epsilon E \rho_E E^\dagger}{1 + 6\epsilon} \quad (19)$$

and

$$\rho_{\text{C,fin}} = \frac{C \rho_C C^\dagger + 6\epsilon \rho_C}{1 + 6\epsilon}. \quad (20)$$

Since $\epsilon \ll 1$, we have $\rho_{\text{C,fin}} \simeq C \rho_C C^\dagger$ and $\rho_{\text{E,fin}} \simeq \rho_E$, consistent with the observation in the experiment of Ref. [3]: The particle leaves a trace at checkpoint C but not at E.

To shine some light on this matter, let us consider what happens when only E is a genuine path-marking operator while A , B , C , and F do not entangle and just introduce phase factors $e^{i\alpha}$, $e^{i\beta}$, $e^{i\gamma}$, and $e^{i\phi}$. Then the final state of Eq. (11) is

$$\rho_{\text{fin}} \propto \left[e^{i\phi} (e^{i\alpha} - e^{i\beta}) E - e^{i\gamma} \right] \rho \left[e^{i\phi} (e^{i\alpha} - e^{i\beta}) E - e^{i\gamma} \right]^\dagger \quad (21)$$

where we leave the normalization implicit. The strength with which E acts is determined by the probability amplitudes $e^{i\phi} e^{i\alpha}$ and $e^{i\phi} e^{i\beta}$ for the paths associated with

checkpoints A and F or B and F, respectively. Their difference is the net amplitude

$$e^{i\phi} (e^{i\alpha} - e^{i\beta}) = 2ie^{i[\phi + \frac{1}{2}(\alpha + \beta)]} \sin \frac{\alpha - \beta}{2}, \quad (22)$$

which vanishes if we have perfect destructive interference at beam splitter BS3 for the particles on the way to BS4. If there is a nonzero relative phase $\frac{1}{2}(\alpha - \beta)$ in the internal loop, operator E does act and the particle leaves a trace at checkpoint E.

This solves the “mystery of the missing trace:” The destructive interference that makes it hard for the particle to reach checkpoint F makes it equally hard to leave a trace at checkpoint E. It is clear, then, that the absence of a trace at checkpoint E does not indicate that the particle did not get there. Rather, it was not given a chance to leave a trace of its passage [44]. A similar observation (for $\epsilon = \frac{1}{3}$) was made by Bartkiewicz *et al.* [13].

There are various manifestations of destructive interference in the three-path interferometer of Fig. 1. The lack of blue probability in Fig. 2 between beam splitters BS3 and BS4 is one, the lack of red probability between BS1 and BS2 is another. We regard the latter as destructive interference of the red amplitudes at BS1; Vaidman would view it as destructive interference of backward-traveling red amplitudes at BS2. From either perspective, there is no mystery unless we choose to mystify the familiar phenomenon of destructive interference.

Accordingly, we improve on Vaidman’s statement that the particle was inside the internal loop but did not enter or leave: The particle was inside but did not leave traces when entering and leaving.

IV. WHICH-PATH KNOWLEDGE

A. Unambiguous path discrimination

In expressions such as ρ_{fin} in Eq. (11), operators E and F always appear together with A or B . No useful information (if any) can be extracted from the path markers at checkpoints E and F that is not already made available at A and B. Therefore, we put $E = F = 1$ and shall only work with A , B , and C .

We can then verify that the path marking works alright by removing beam splitters BS3 and BS4 and using three detectors, one at each output port; see Fig. 4. The matrices for the unitary operators U_3 and U_4 of Eq. (1) are here replaced by

$$U_3 = \begin{pmatrix} 0 & 1 & 0 \\ 1 & 0 & 0 \\ 0 & 0 & 1 \end{pmatrix}, \quad U_4 = \begin{pmatrix} 1 & 0 & 0 \\ 0 & 0 & 1 \\ 0 & 1 & 0 \end{pmatrix}. \quad (23)$$

Just before the particle is detected, the joint state of the

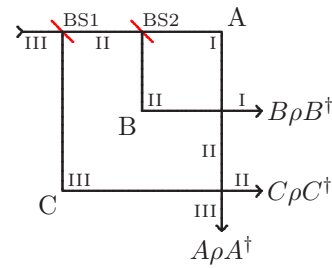


FIG. 4. Marking the path through the interferometer. Unitary operators A , B , and C are acting on the path-marker degrees of freedom when the particle passes through the respective checkpoints A, B, or C. Here, beam splitters BS3 and BS4 are removed, and the conditional states of the path marker are indicated at the exit ports: $A\rho A^\dagger$, $B\rho B^\dagger$, and $C\rho C^\dagger$ for the paths through checkpoint A, B, or C, respectively, where ρ is the initial state of the path marker.

particle and the path marker is

$$\frac{1}{3} \begin{pmatrix} B \\ C \\ A \end{pmatrix} \rho \begin{pmatrix} B \\ C \\ A \end{pmatrix}^\dagger. \quad (24)$$

The diagonal elements of the three-by-three matrix for the path degree of freedom — these are $\frac{1}{3}B\rho B^\dagger$, $\frac{1}{3}C\rho C^\dagger$, and $\frac{1}{3}A\rho A^\dagger$ — are the unnormalized final path-marker states conditioned on detecting the particle at exits I, II, or III, respectively, after passing the corresponding checkpoint B, C, or A. The traces of these diagonal elements are the respective probabilities, each equal to one-third. We acquire which-path knowledge by a measurement on the path-marker degrees of freedom that distinguishes between the states $A\rho A^\dagger$, $B\rho B^\dagger$, and $C\rho C^\dagger$, which label the corresponding exit ports in Fig. 4.

It is important that there is an operational confirmation of the which-path knowledge thus gained. For this purpose, one experimenter (Alice) takes note which of the three detectors found the particle, and a second experimenter (Bob) examines the path marker to find out which checkpoint was visited. Bob has various strategies at his disposal, among them two particularly important ones.

In the first strategy, Bob makes an educated guess about each particle’s path and maximizes his chance of guessing right. For this purpose, he employs the so-called *minimum-error measurement* [45], and will guess right as often as possible without, however, being sure about even one particle’s path. In the second strategy, he wants to be absolutely sure about the paths of some particles at the expense of having no clue which path was taken by the other particles, and chooses his measurement such that the fraction of particles with surely-known paths is as large as possible. The *measurement for unambiguous discrimination* [46–49] serves this purpose.

In the present context of “asking particles where they have been” (paraphrasing the title of Ref. [3]), unambigu-

ous path knowledge is, as we will see, the most useful and, therefore, Bob chooses the second strategy. After performing the unambiguous discrimination of the path-marker states $A\rho A^\dagger$, $B\rho B^\dagger$, and $C\rho C^\dagger$, he places a bet on one of the three cases whenever he is sure which checkpoint was visited. If Bob wins all his bets, the path marker works correctly and the stored which-path information is correctly extracted.

For the sake of simplicity and clarity of presentation, we assume that the initial path-marker state is pure and describe it by a wave function ψ , $\rho \hat{=} \psi\psi^\dagger$. The action of A , B , or C yields corresponding wave functions ψ_A , ψ_B , or ψ_C , each slightly different from ψ , in accordance with

$$A\rho A^\dagger \hat{=} \psi_A\psi_A^\dagger, \quad B\rho B^\dagger \hat{=} \psi_B\psi_B^\dagger, \quad C\rho C^\dagger \hat{=} \psi_C\psi_C^\dagger. \quad (25)$$

Following Vaidman [1], the ‘‘pointer variables’’ at checkpoints A , B , and C are in the same initial state, with which we associate the wave function χ_0 , and the unitary operators A , B , and C have the same effect on their respective pointers, changing χ_0 to χ_ϵ . Accordingly, we have the wave function $\psi = \chi_0 \otimes \chi_0 \otimes \chi_0$ for the initial path-marker state, and the final wave functions are

$$\begin{aligned} \psi_A &= \chi_\epsilon \otimes \chi_0 \otimes \chi_0, \\ \psi_B &= \chi_0 \otimes \chi_\epsilon \otimes \chi_0, \\ \psi_C &= \chi_0 \otimes \chi_0 \otimes \chi_\epsilon. \end{aligned} \quad (26)$$

The expectation values of Eq. (17),

$$\left. \begin{aligned} \langle A \rangle &= \text{tr}\{\psi_A\psi^\dagger\} \\ \langle B \rangle &= \text{tr}\{\psi_B\psi^\dagger\} \end{aligned} \right\} = \chi_0^\dagger \chi_\epsilon (\chi_0^\dagger \chi_0)^2 = \chi_0^\dagger \chi_\epsilon, \quad (27)$$

establish $\chi_0^\dagger \chi_\epsilon = \sqrt{1-3\epsilon}$, so that

$$\psi_a^\dagger \psi_b = 1 - 3\epsilon + 3\epsilon\delta_{ab} \quad \text{for } a,b=A,B,C, \quad (28)$$

which confirms that checkpoints A , B , and C are on equal footing. We note that $(\psi_B - \psi_A)^\dagger \psi_C = 0$ is a consequence of the symmetric way of treating the three checkpoints.

Since only the three wave functions ψ_A , ψ_B , and ψ_C are involved, we can use three-component columns for them. A specific choice is

$$\left. \begin{aligned} \psi_A \\ \psi_B \end{aligned} \right\} = \begin{bmatrix} \pm\sqrt{3\epsilon/2} \\ -\sqrt{\epsilon/2} \\ \sqrt{1-2\epsilon} \end{bmatrix}, \quad \psi_C = \begin{bmatrix} 0 \\ \sqrt{2\epsilon} \\ \sqrt{1-2\epsilon} \end{bmatrix}, \quad (29)$$

where we use square parentheses for the columns of the path-marker wave functions to avoid confusion with the columns for the particle’s path amplitudes, such as the columns in Eq. (24).

The error-minimizing measurement would allow Bob to guess right for a fraction $\frac{1}{3}(\sqrt{1-2\epsilon} + 2\sqrt{\epsilon})^2$ of the particles [50] while never being certain about the path. But he wants to know the path for sure before placing his bet and, therefore, he employs the measurement for

unambiguous discrimination with the outcome operators $\Pi_a = \phi_a\phi_a^\dagger$ for the three cases $a=A, B, \text{ or } C$ and $\Pi_0 = \phi_0\phi_0^\dagger$ for the inconclusive outcome, where [47, 50]

$$\left. \begin{aligned} \phi_A \\ \phi_B \end{aligned} \right\} = \begin{bmatrix} \pm\sqrt{1/2} \\ -\sqrt{1/6} \\ \sqrt{\epsilon/(3-6\epsilon)} \end{bmatrix}, \quad \phi_C = \begin{bmatrix} 0 \\ \sqrt{2/3} \\ \sqrt{\epsilon/(3-6\epsilon)} \end{bmatrix} \quad (30)$$

and

$$\phi_0 = \sqrt{\frac{1-3\epsilon}{1-2\epsilon}} \begin{bmatrix} 0 \\ 0 \\ 1 \end{bmatrix}. \quad (31)$$

We have

$$\begin{aligned} \text{tr}\{\Pi_a\psi_b\psi_b^\dagger\} &= |\phi_a^\dagger\psi_b|^2 = 3\epsilon\delta_{ab} \quad \text{for } a,b=A,B,C, \\ \text{tr}\{\Pi_0\psi_a\psi_a^\dagger\} &= 1 - 3\epsilon \quad \text{for } a=A,B,C, \end{aligned} \quad (32)$$

which tell us that Bob gets the inconclusive result for a fraction of $1-3\epsilon$ of the particles, and then he has no clue about the path, and does not place a bet. For the remaining fraction of 3ϵ , he knows the path for sure and wins his bet [51]. As expected, the weak path marking ($\epsilon \ll 1$) does not store much which-path information in the final path-marker state.

Here, then, is a more detailed account of the betting game alluded to above. The source emits a particle into the interferometer and the unitary operators A , B , and C , acting at checkpoints A , B , and C , respectively, entangle the path qutrit of the particle with the marker degrees of freedom, on which Bob performs the measurement of unambiguous discrimination. He either gets the inconclusive result, in which case he does nothing, or he finds one of the three conclusive results and then bets on the respective path (‘‘I bet that the particle went through checkpoint B ,’’ say).

Whenever Alice verifies the path, be it by the setup of Fig. 4 or otherwise, she will confirm that Bob identified the actual path correctly. This establishes, in a definite operational sense, that Bob’s conclusive results are in a strict one-to-one correlation with the particle’s path through the interferometer. In this procedure, it does not matter whether Alice first detects the particle and Bob later performs the unambiguous discrimination, or they do it in the reverse temporal order.

With beam splitters $BS3$ and $BS4$ in place, the final state of the path marker, conditioned on detecting the particle by D , is that of Eq. (11),

$$\rho_{\text{fin}} = \frac{1}{1+6\epsilon} (\psi_C + \psi_B - \psi_A)(\psi_C + \psi_B - \psi_A)^\dagger. \quad (33)$$

The conclusive outcomes of Bob’s measurement for unambiguous discrimination occur with equal probability,

$$\text{tr}\{\Pi_a\rho_{\text{fin}}\} = \frac{3\epsilon}{1+6\epsilon} \quad \text{for } a=A,B,C, \quad (34)$$

and

$$\text{tr}\{\Pi_0\rho_{\text{fin}}\} = \frac{1-3\epsilon}{1+6\epsilon} \quad (35)$$

is the conditional probability of getting the inconclusive outcome. The equal probabilities of Eq. (34) are reminiscent of the equal heights of the three peaks in Fig. 3.

Do these equal probabilities tell us that one-third of the particles went through checkpoint A on the way from the source to the detector, another one-third through checkpoint B, and the remaining one-third through checkpoint C? No. This statement is correct only for those particles for which Bob obtains definite path knowledge, which is the very small fraction $\frac{9\epsilon}{1+6\epsilon}$ of all particles. Bob cannot say anything about the vast majority of the particles, for which he gets the inconclusive outcome.

It is not possible to invoke a fair-sampling assumption here (which is, however, an implicit assumption in Ref. [3]; see also [19]) and so infer that the particles with unknown path are as equally distributed over the three paths as those with a known path. But it is possible to argue that Bob gets the inconclusive result for particles that went through checkpoint C.

B. An accounting exercise

This argument has two ingredients. First, we observe that an interferometer phase φ introduced at checkpoint C, i.e., replace ψ_C by $e^{i\varphi}\psi_C$ in Eq. (33), does not change the probability that the next particle is detected by D,

$$\begin{aligned} & \langle T_{\text{fin}}^\dagger T_{\text{fin}} \rangle \\ &= \frac{1}{9} \text{tr} \left\{ (e^{i\varphi}\psi_C + \psi_B - \psi_A)(e^{i\varphi}\psi_C + \psi_B - \psi_A)^\dagger \right\} \\ &= \frac{1}{9} \psi_C^\dagger \psi_C + \frac{1}{9} (\psi_B - \psi_A)^\dagger (\psi_B - \psi_A) = \frac{1+6\epsilon}{9}, \quad (36) \end{aligned}$$

where $(\psi_B - \psi_A)^\dagger \psi_C = 0$ enters. It follows that the amplitudes that reach beam splitter BS4 from checkpoint C and BS3 are incoherent. We must, therefore, add the probabilities rather than the probability amplitudes.

Second, the probabilities of reaching beam splitter BS4 are $\frac{1}{3}$ (for path C \rightarrow BS4) and ϵ (for path BS3 \rightarrow BS4), and the reflection and transmission probabilities of BS4 are $\frac{1}{3}$ and $\frac{2}{3}$, respectively. Indeed, the resulting probability

$$\frac{1}{3} \times \frac{1}{3} + \frac{2}{3} \times \epsilon = \frac{1+6\epsilon}{9} \quad (37)$$

agrees with that in Eq. (36), with $\frac{1}{9}$ associated with checkpoint C and $\frac{6\epsilon}{9}$ with the internal loop. The corresponding fractions are

$$\frac{1}{1+6\epsilon} = \frac{1-3\epsilon}{1+6\epsilon} + \frac{3\epsilon}{1+6\epsilon} \quad \text{for path C}\rightarrow\text{BS4} \quad (38)$$

and

$$\frac{6\epsilon}{1+6\epsilon} = \frac{3\epsilon}{1+6\epsilon} + \frac{3\epsilon}{1+6\epsilon} \quad \text{for path BS3}\rightarrow\text{BS4}. \quad (39)$$

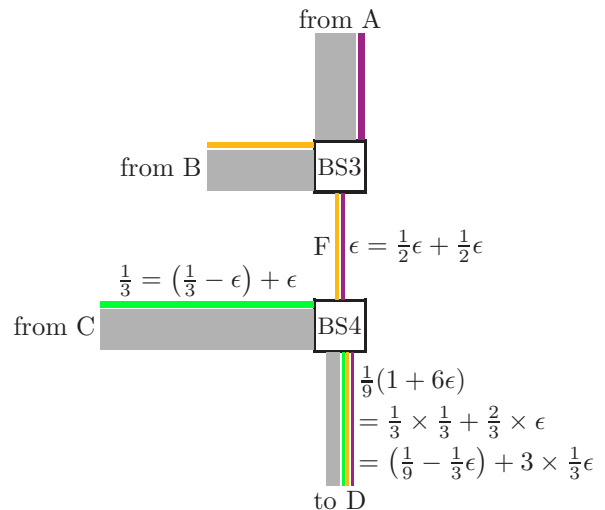


FIG. 5. Unambiguous path knowledge about particles detected by detector D. The next particle to enter the three-path interferometer is detected with probability $\frac{1}{9}(1+6\epsilon)$; see Eq. (36). On the way to detector D, the particle either passes checkpoint C with probability $\frac{1}{3}$ and then has a $\frac{1}{3}$ chance of being reflected by beam splitter BS4, or it passes F with probability ϵ and then has a $\frac{2}{3}$ chance of being transmitted by BS4. The conclusive outcomes (purple, orange, green) of the unambiguous path discrimination *for these particles detected by D* identify the paths via checkpoints A, B, or C with equal probability of $\frac{1}{3}\epsilon/\frac{1}{9}(1+6\epsilon)$; see Eq. (34). Since that fully accounts for the particles that took the path BS3 \rightarrow BS4 \rightarrow D, the inconclusive measurement outcomes (gray) surely identify particles that followed the path C \rightarrow BS4 \rightarrow D. In the limit $\epsilon \rightarrow 0$, all particles reach D via C. The intensities at the other exit ports — exit I from BS3 and exit II from BS4 — are not indicated in the figure.

The fraction for path BS3 \rightarrow BS4 is fully accounted for by the conclusive outcomes for checkpoints A and B in Eq. (34), and the fraction for path C \rightarrow BS4 is the sum of the fraction for the conclusive outcome C and the fraction for the inconclusive outcome in Eq. (35). This accounting exercise suggests strongly that the fraction $\frac{1-3\epsilon}{1+6\epsilon}$ of Bob's inconclusive outcomes is associated with particles that passed checkpoint C. If this were indeed so, all particles detected by D would have gone by checkpoint C in the limit of $\epsilon \rightarrow 0$, fully consistent with the common-sense reading of Fig. 2. The matter is summarized in Fig. 5.

We emphasize the great benefit of the unambiguous path discrimination by the measurement with the outcomes Π_A , Π_B , Π_C , and Π_0 of Eqs. (30) and (31): While the inconclusive outcome Π_0 yields no path information for the whole ensemble of particles emitted by the source S, it provides definite path knowledge (via checkpoint C, that is) for the subensemble of particles detected by detector D; more about this in the next section. All of the pre-selected and post-selected particles of interest have a known path through Vaidman's interferometer. We ask these particles where they have been, and they all give a definite answer.

Whether one finds this reasoning convincing or regards it as another appeal to common sense of no consequence, it is certainly the case that the outcomes Π_A and Π_B account fully for the fraction of particles that reach beam splitter BS4 via checkpoints A or B. How do we reconcile the definitely known paths with the destructive interference at BS3? True, destructive interference is only possible if the path cannot be known and, yet, there is no contradiction here, as we shall see in Sec. VI.

In passing, we note another consequence of the lack of coherence between the amplitudes for paths BS3→BS4 and C→BS4. If we block the path from checkpoint C to beam splitter BS4 (or, equivalently, remove the entrance beam splitter BS1), then we get a signal with a strength proportional to ϵ at detector D. This is in marked contrast to the experiment of Danan *et al.* [3], where the corresponding amplitudes are coherent — the electric field vectors of the arriving partial beams just add to yield the fields of the emerging beams — and, therefore, the power spectrum in their Fig. 2(b) is proportional to their analog of ϵ while that in Fig. 2(c) is proportional to ϵ^2 and buried in the noise; Fig. 4 in [22] illustrates this point.

C. Sorted subensembles

At an instant after unitary operators A , B , C acted when the particle passed checkpoints A, B, C and before the path amplitudes are processed by beam splitters BS3 and BS4, the entangled state of the path marker and the particle has the wave function

$$\begin{aligned} & \frac{1}{\sqrt{3}} \left[\psi_A \otimes \begin{pmatrix} 1 \\ 0 \\ 0 \end{pmatrix} + \psi_B \otimes \begin{pmatrix} 0 \\ 1 \\ 0 \end{pmatrix} + \psi_C \otimes \begin{pmatrix} 0 \\ 0 \\ 1 \end{pmatrix} \right] \\ &= \frac{1}{\sqrt{3}} \begin{pmatrix} \psi_A \\ \psi_B \\ \psi_C \end{pmatrix}. \end{aligned} \quad (40)$$

Upon performing his measurement for unambiguous path discrimination, Bob sorts the particles into subensembles in accordance with the outcome he observes [52]. The density matrices for the subensembles with known paths (purple, orange, green in Fig. 5),

$$\frac{1}{3} \begin{pmatrix} \phi_a^\dagger \psi_A \\ \phi_a^\dagger \psi_B \\ \phi_a^\dagger \psi_C \end{pmatrix} \begin{pmatrix} \phi_a^\dagger \psi_A \\ \phi_a^\dagger \psi_B \\ \phi_a^\dagger \psi_C \end{pmatrix}^\dagger = \frac{1}{3} \phi_a^\dagger \begin{pmatrix} \psi_A \\ \psi_B \\ \psi_C \end{pmatrix} \begin{pmatrix} \psi_A \\ \psi_B \\ \psi_C \end{pmatrix}^\dagger \phi_a \quad (41)$$

for $a=A,B,C$, are rank-one projectors on their respective paths with

$$\frac{1}{\sqrt{3}} \phi_a^\dagger \begin{pmatrix} \psi_A \\ \psi_B \\ \psi_C \end{pmatrix} = \sqrt{\epsilon} \begin{pmatrix} 1 \\ 0 \\ 0 \end{pmatrix},$$

$$\begin{aligned} \frac{1}{\sqrt{3}} \phi_B^\dagger \begin{pmatrix} \psi_A \\ \psi_B \\ \psi_C \end{pmatrix} &= \sqrt{\epsilon} \begin{pmatrix} 0 \\ 1 \\ 0 \end{pmatrix}, \\ \frac{1}{\sqrt{3}} \phi_C^\dagger \begin{pmatrix} \psi_A \\ \psi_B \\ \psi_C \end{pmatrix} &= \sqrt{\epsilon} \begin{pmatrix} 0 \\ 0 \\ 1 \end{pmatrix}; \end{aligned} \quad (42)$$

the strict one-to-one correspondence between Bob's outcome and the particle's path is manifest here. We keep the probability amplitudes of $\sqrt{\epsilon}$ as overall factors in the particle wave functions to remind us of the statistical weights of the subensembles, as indicated by the thickness of the purple, orange, and green lines in Fig. 5.

These three subensembles of particles with operationally known paths are supplemented by the fourth subensemble for Bob's inconclusive outcome (gray in Fig. 5). Its density matrix is also a rank-one projector with the wave function

$$\frac{1}{\sqrt{3}} \phi_0^\dagger \begin{pmatrix} \psi_A \\ \psi_B \\ \psi_C \end{pmatrix} = \sqrt{\frac{1-3\epsilon}{3}} \begin{pmatrix} 1 \\ 1 \\ 1 \end{pmatrix}, \quad (43)$$

which is exactly the $\epsilon = 0$ wave function of particles that are not monitored while traversing the three-path interferometer [cf. Eq. (A.6)], multiplied by the probability amplitude $\sqrt{1-3\epsilon}$ for the inconclusive outcome. No path knowledge is available for the particles in this subensemble.

The wave functions in Eqs. (40), (42), and (43) apply before the particle reaches beam splitter BS3. The wave functions after BS3 and before BS4 are

$$U_3 \frac{1}{\sqrt{3}} \begin{pmatrix} \psi_A \\ \psi_B \\ \psi_C \end{pmatrix} = \frac{1}{\sqrt{6}} \begin{pmatrix} \psi_B + \psi_A \\ \psi_B - \psi_A \\ \sqrt{2} \psi_C \end{pmatrix} \quad (44)$$

for the entangled marker-particle state, and

$$\frac{1}{\sqrt{6}} \phi_x^\dagger \begin{pmatrix} \psi_B + \psi_A \\ \psi_B - \psi_A \\ \sqrt{2} \psi_C \end{pmatrix} \quad \text{for } x=A,B,C, \text{ or } 0 \quad (45)$$

for the conditional particle states. In view of the eventual conditioning on particles detected by detector D, we focus on the components that are processed by beam splitter BS4 and project out the then irrelevant path-I component,

$$\begin{pmatrix} 0 & 0 & 0 \\ 0 & 1 & 0 \\ 0 & 0 & 1 \end{pmatrix} \frac{1}{\sqrt{6}} \phi_x^\dagger \begin{pmatrix} \psi_B + \psi_A \\ \psi_B - \psi_A \\ \sqrt{2} \psi_C \end{pmatrix} = \begin{pmatrix} 0 \\ \frac{1}{\sqrt{6}} \phi_x^\dagger (\psi_B - \psi_A) \\ \frac{1}{\sqrt{3}} \phi_x^\dagger \psi_C \end{pmatrix} \quad (46)$$

and so arrive at the conditional wave functions for the four subensembles, namely

$$\sqrt{\frac{\epsilon}{2}} \begin{pmatrix} 0 \\ -1 \\ 0 \end{pmatrix}, \quad \sqrt{\frac{\epsilon}{2}} \begin{pmatrix} 0 \\ 1 \\ 0 \end{pmatrix}, \quad \sqrt{\epsilon} \begin{pmatrix} 0 \\ 0 \\ 1 \end{pmatrix} \quad (47)$$

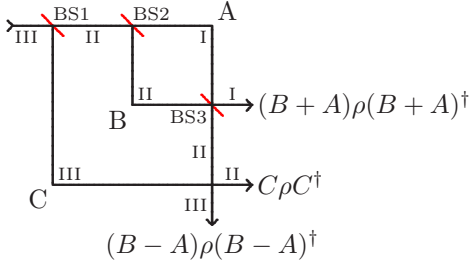


FIG. 6. Marking the path through the interferometer as in Fig. 4. Now, beam splitter BS3 is in place but BS4 is still removed. The conditional states of the marker degrees of freedom are $(B+A)\rho(B+A)^\dagger$, $C\rho C^\dagger$, and $(B-A)\rho(B-A)^\dagger$, respectively, upon detecting the particle at exit I, II, or III.

for $x=A, B$, and C , respectively, and

$$\sqrt{\frac{1-3\epsilon}{3}} \begin{pmatrix} 0 \\ 0 \\ 1 \end{pmatrix} \quad (48)$$

for the inconclusive outcome. This confirms the conclusion reached by the accounting exercise of Sec. IV B: Whenever Bob obtains the inconclusive outcome for a particle detected by detector D, then this particle has arrived at beam splitter BS4 along path III, i.e., via checkpoint C [53].

Finally, for the record, the entangled marker-particle state at the exit stage of the three-path interferometer — before the particle is detected at exit I, II, or III — is

$$U_4 U_3 \frac{1}{\sqrt{3}} \begin{pmatrix} \psi_A \\ \psi_B \\ \psi_C \end{pmatrix} = \begin{pmatrix} \frac{1}{\sqrt{6}}(\psi_B + \psi_A) \\ \frac{1}{\sqrt{18}}(2\psi_C - \psi_B + \psi_A) \\ \frac{1}{3}(\psi_C + \psi_B - \psi_A) \end{pmatrix}, \quad (49)$$

and the particle wave functions associated with the paths through checkpoints A, B, and C are

$$\sqrt{\frac{\epsilon}{6}} \begin{pmatrix} \sqrt{3} \\ 1 \\ -\sqrt{2} \end{pmatrix}, \quad \sqrt{\frac{\epsilon}{6}} \begin{pmatrix} \sqrt{3} \\ -1 \\ \sqrt{2} \end{pmatrix}, \quad \sqrt{\frac{\epsilon}{3}} \begin{pmatrix} 0 \\ \sqrt{2} \\ 1 \end{pmatrix}, \quad (50)$$

respectively, while the wave function

$$\frac{1}{3}\sqrt{1-3\epsilon} \begin{pmatrix} \sqrt{6} \\ \sqrt{2} \\ 1 \end{pmatrix} \quad (51)$$

applies to the particles with unknown path. Alice can check which one is the actual path by an interferometric measurement that discriminates between the three orthogonal wave functions in Eq. (50). This is an example of the “otherwise” in the betting game between Eqs. (32) and (33).

V. MORE WHICH-PATH KNOWLEDGE

Bob’s measurement with the outcome operators specified by Eqs. (30) and (31) distinguishes between the three possible detection events of the setup in Fig. 4. In view of Eq. (36), it appears to be more useful to tell apart the three detection events of the setup in Fig. 6, where beam splitter BS3 is in place while BS4 is not. Alice and Bob then play the betting game described between Eqs. (32) and (33), with the necessary modifications as they follow from

$$\frac{1}{6} \begin{pmatrix} B+A \\ \sqrt{2}C \\ B-A \end{pmatrix} \rho \begin{pmatrix} B+A \\ \sqrt{2}C \\ B-A \end{pmatrix}^\dagger \quad (52)$$

for the joint state of the particle and the path marker instead of the state in Eq. (24).

Here, Bob’s task is to discriminate between the three path-marker states

$$\left. \begin{aligned} \rho_I \\ \rho_{III} \end{aligned} \right\} \propto (B \pm A)\rho(B \pm A)^\dagger = (\psi_B \pm \psi_A)(\psi_B \pm \psi_A)^\dagger, \\ \rho_{II} \propto C\rho C^\dagger = \psi_C\psi_C^\dagger, \quad (53)$$

which have a priori probabilities of occurrence of

$$\begin{aligned} \frac{1}{6}\text{tr}\{(B \pm A)\rho(B \pm A)^\dagger\} &= \begin{cases} \frac{1}{3}(2-3\epsilon), \\ \epsilon, \end{cases} \\ \frac{2}{6}\text{tr}\{C\rho C^\dagger\} &= \frac{1}{3}, \end{aligned} \quad (54)$$

respectively [cf. Eq. (44)]. Much more useful than discriminating between ρ_I , ρ_{II} , and ρ_{III} , however, is a measurement that tells ρ_{II} and ρ_{III} apart because ρ_I is irrelevant for the particles detected by detector D in the full setup of Fig. 1 with beam splitter BS4 in place. Accordingly, the appropriate verification protocol is this: Alice takes note of the particles detected at exits II and III in the setup of Fig. 6, and challenges Bob to place a bet.

Since $(\psi_B - \psi_A)^\dagger \psi_C = 0$, Bob uses an orthogonal measurement where the outcome operators $\Pi_j = \phi_j \phi_j^\dagger$ for $j = I, II, III$ project on

$$\begin{aligned} \phi_I &= \begin{bmatrix} 0 \\ -\sqrt{1-2\epsilon} \\ \sqrt{2\epsilon} \end{bmatrix} = \frac{\psi_A + \psi_B - 2(1-3\epsilon)\psi_C}{3\sqrt{2\epsilon}(1-2\epsilon)}, \\ \phi_{II} &= \begin{bmatrix} 0 \\ \sqrt{2\epsilon} \\ \sqrt{1-2\epsilon} \end{bmatrix} = \psi_C, \\ \phi_{III} &= \begin{bmatrix} 1 \\ 0 \\ 0 \end{bmatrix} = \frac{\psi_A - \psi_B}{\sqrt{6\epsilon}}, \end{aligned} \quad (55)$$

which are such that

$$\begin{aligned} \text{tr}\{\Pi_I\rho_{II}\} &= 0, & \text{tr}\{\Pi_I\rho_{III}\} &= 0, \\ \text{tr}\{\Pi_{II}\rho_{II}\} &= 1, & \text{tr}\{\Pi_{II}\rho_{III}\} &= 0, \\ \text{tr}\{\Pi_{III}\rho_{II}\} &= 0, & \text{tr}\{\Pi_{III}\rho_{III}\} &= 1. \end{aligned} \quad (56)$$

It follows that Bob will never get outcome I; he bets on exit II when he gets outcome II, and on exit III for outcome III. As there are no inconclusive measurement outcomes, Bob will place a bet for every particle detected by Alice in exit II or exit III, and he wins all bets. That is: He knows for sure, for each and every particle, whether it went through checkpoint C (outcome II) or took the route through the internal loop (outcome III).

Now, with beam splitter BS4 back in place, Bob examines the final path-marker state of Eq. (33) and he gets outcomes I, II, III with the probabilities

$$\begin{aligned} \text{tr}\{\Pi_I\rho_{\text{fin}}\} &= 0, \\ \text{tr}\{\Pi_{II}\rho_{\text{fin}}\} &= \frac{1}{1+6\epsilon}, \\ \text{tr}\{\Pi_{III}\rho_{\text{fin}}\} &= \frac{6\epsilon}{1+6\epsilon}. \end{aligned} \quad (57)$$

As we know, the particle's probability amplitudes processed by beam splitter BS4 refer to known paths — this is the essence of Eq. (56) — and, therefore, they are incoherent and we add the probabilities rather than the probability amplitudes. As we did in Eq. (37), we account for the reflection and transmission probabilities of BS4, establish the a priori probabilities of being detected by D as $\frac{1}{9}$ and $\frac{2}{3}\epsilon$ for the particle arriving via checkpoint C or the internal loop, respectively, and so confirm that the probabilities in Eq. (57) are the correct relative frequencies,

$$\frac{1}{1+6\epsilon} = \frac{\frac{1}{9}}{\frac{1}{9} + \frac{2}{3}\epsilon}, \quad \frac{6\epsilon}{1+6\epsilon} = \frac{\frac{2}{3}\epsilon}{\frac{1}{9} + \frac{2}{3}\epsilon}. \quad (58)$$

In the limit $\epsilon \rightarrow 0$, Bob gets outcome II for every particle, i.e., every particle arrives at detector D via checkpoint C. This is exactly what common sense tells us.

This confirms once more our conclusions reached by the accounting exercise of Sec. IV B and the sorted-subensembles argument of Sec. IV C: In the measurement of Eqs. (30) and (31), all inconclusive results are obtained for particles that passed checkpoint C before reaching detector D; this measurement, then, provides full path knowledge for every particle detected by D. The extrapolation $\epsilon \rightarrow 0$ supports the common-sense conclusion in Sec. II, which simply recognizes that there is only one blue path from source S to detector D in Fig. 2.

With regard to the final path-marker wave function in Eq. (33), these considerations establish that we should read it as the superposition of the normalized wave functions ψ_C for the path $C \rightarrow \text{BS4} \rightarrow D$ and $(\psi_B - \psi_A)/\sqrt{6\epsilon}$ for the path $\text{BS3} \rightarrow \text{BS4} \rightarrow D$, that is

$$\frac{1}{\sqrt{1+6\epsilon}}(\psi_C + \psi_B - \psi_A)$$

$$= \frac{1}{\sqrt{1+6\epsilon}}\psi_C + \sqrt{\frac{6\epsilon}{1+6\epsilon}}\frac{\psi_B - \psi_A}{\sqrt{6\epsilon}}. \quad (59)$$

Since $\psi_C = \phi_{II}$ and $\psi_B - \psi_A = -\sqrt{6\epsilon}\phi_{III}$ are orthogonal, this superposition refers to fully distinguishable alternatives [see Eq. (57)], and in the limit of $\epsilon \rightarrow 0$ there is only the path $C \rightarrow \text{BS4} \rightarrow D$.

VI. TWO-PATH INTERFEROMETER WITH WEAK PATH MARKING

We return to the question raised at the end of Sec. IV and focus on the two-path interferometer of the internal loop. The scheme of a two-path experiment is sketched in Fig. 7(a) where the unitary matrix for beam splitters BS2 and BS3 is that of Eq. (1), only that we ignore the third row and column in the present context, so that

$$U_2 = U_3 = \frac{1}{\sqrt{2}} \begin{pmatrix} 1 & 1 \\ -1 & 1 \end{pmatrix} \quad (60)$$

here. For the path marking, too, we now use a binary degree of freedom (“qubit”) and represent the unitary operators A and B as well as the initial path-marker state ρ by two-by-two matrices. In particular, we choose

$$\begin{aligned} \left. \begin{aligned} A\rho A^\dagger \\ B\rho B^\dagger \end{aligned} \right\} &\hat{=} \begin{bmatrix} \sqrt{1-\epsilon} \\ \mp\sqrt{\epsilon} \end{bmatrix} \begin{bmatrix} \sqrt{1-\epsilon} \\ \mp\sqrt{\epsilon} \end{bmatrix}^\dagger, \\ A\rho B^\dagger &\hat{=} \begin{bmatrix} \sqrt{1-\epsilon} \\ -\sqrt{\epsilon} \end{bmatrix} \begin{bmatrix} \sqrt{1-\epsilon} \\ \sqrt{\epsilon} \end{bmatrix}^\dagger, \end{aligned} \quad (61)$$

where ϵ is the probability that the next particle emitted by source S will reach detector D,

$$\epsilon = \text{tr}\left\{T_{\text{fin}}\rho T_{\text{fin}}^\dagger\right\} \quad (62)$$

with $T_{\text{fin}} = \frac{1}{2}(B - A)$. After detecting the particle, the conditional final state of the path-marker qubit is

$$\rho_{\text{fin}} = \frac{1}{\epsilon}T_{\text{fin}}\rho T_{\text{fin}}^\dagger \hat{=} \begin{bmatrix} 0 & 0 \\ 0 & 1 \end{bmatrix}. \quad (63)$$

Figure 7(b) depicts the situation with beam splitter BS3 removed, in which we implement the analog of the protocol for Fig. 4: Alice records whether the particle took exit I or exit II, and Bob measures the path-marker qubit and then places a bet. His measurement for unambiguous discrimination has the outcome operators

$$\left. \begin{aligned} \Pi_A \\ \Pi_B \end{aligned} \right\} \hat{=} \frac{1}{2} \begin{bmatrix} \frac{\epsilon}{1-\epsilon} & \mp\sqrt{\frac{\epsilon}{1-\epsilon}} \\ \mp\sqrt{\frac{\epsilon}{1-\epsilon}} & 1 \end{bmatrix} \quad (64)$$

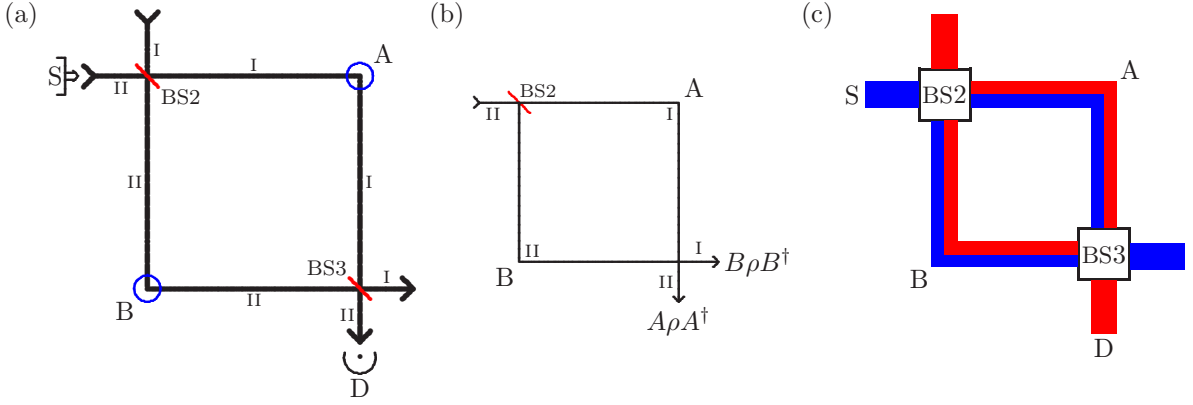


FIG. 7. Two-path interferometer. (a) Particles are emitted from source S, detected by detector D, and pass checkpoints A or B on the way from S to D. (b) Beam splitter BS3 is removed for the verification that the discrimination between the final path-marker states $A\rho A^\dagger$ and $B\rho B^\dagger$ correctly identifies the paths via checkpoints A and B. (c) In this analog of Fig. 2, the blue lines indicate the probabilities for the particles that surely emerged from source S, and the red lines are for the particles that will surely be detected by detector D.

for the paths identified by checkpoints A and B, and

$$\Pi_0 \hat{=} \frac{1-2\epsilon}{1-\epsilon} \begin{bmatrix} 1 & 0 \\ 0 & 0 \end{bmatrix} \quad (65)$$

for the inconclusive measurement. Bob places a bet for every conclusive outcome (fraction 2ϵ of all cases) and wins all the bets. He does not bet on the exit when he gets the inconclusive outcome (fraction $1-2\epsilon$).

With beam splitter BS3 in place and the particle detected by D at exit II, Bob's outcome probabilities are

$$\begin{aligned} p_A &= \text{tr}\{\Pi_A \rho_{\text{fin}}\} = \frac{1}{2}, \\ p_B &= \text{tr}\{\Pi_B \rho_{\text{fin}}\} = \frac{1}{2}, \\ p_0 &= \text{tr}\{\Pi_0 \rho_{\text{fin}}\} = 0. \end{aligned} \quad (66)$$

Since there are no inconclusive outcomes, Bob knows for *every* particle detected by D whether it went through checkpoint A or checkpoint B on its way from the source to the detector.

If, rather than detecting the particle at exit II, we detect it at exit I, which will happen with probability $1-\epsilon$ for the next particle, the conditional final state of the path marker is

$$\rho'_{\text{fin}} = \frac{1}{1-\epsilon} \frac{B+A}{2} \rho \frac{(B+A)^\dagger}{2} \hat{=} \begin{bmatrix} 1 & 0 \\ 0 & 0 \end{bmatrix}, \quad (67)$$

and Bob obtains his measurement outcomes with the probabilities

$$p'_A = p'_B = \frac{1}{2} \frac{\epsilon}{1-\epsilon} \quad \text{and} \quad p'_0 = \frac{1-2\epsilon}{1-\epsilon}. \quad (68)$$

That is: The small fraction $\frac{\epsilon}{1-\epsilon} \simeq \epsilon$ of the particles that take exit I have a known path through the interferometer while the path is unknown for the vast majority of

the particles (fraction $\frac{1-2\epsilon}{1-\epsilon} \simeq 1-\epsilon$). These particles with unknown, and unknowable, paths exhibit interference — perfect constructive interference for exit I, perfect destructive interference for exit II.

Accordingly, we have this full picture for the particles observed after exiting from the interferometer: A fraction $p_A\epsilon + p'_A(1-\epsilon) = \epsilon$ of all particles passed checkpoint A and half of them emerged from exit I, the other half from exit II. Another fraction $p_B\epsilon + p'_B(1-\epsilon) = \epsilon$ surely passed checkpoint B and half of them took exit I, the other half exit II. The remaining fraction $p_0\epsilon + p'_0(1-\epsilon) = 1-2\epsilon$ consists entirely of particles with unknowable paths through the interferometer and full interference strength; they all emerged from exit I.

We can change the distribution of the interfering particles between the exits by introducing a phase φ into the interferometer — formally by the replacement $A\rho B^\dagger \rightarrow e^{i\varphi}A\rho B^\dagger$ in Eq. (61). Then we observe interference fringes with a visibility of $1-2\epsilon$.

Here, then, is the answer to the question asked in the next-to-last paragraph of Sec. IV B: The particles that pass checkpoint F in the three-path interferometer of Fig. 1 do not participate in the interference; all the interfering particles take exit I at beam splitter BS3. There really is no contradiction.

We arrive at this full picture thanks to the which-path information acquired by the unambiguous path discrimination, which enables us to sort the particles into subensembles with either a surely-known path or an unknowable path. The error-minimizing measurement would provide information of another kind that is useful for its own purpose but does not yield a definite answer when “asking particles where they have been.”

As a final remark we note that the analog of Fig. 2 in Fig. 7(c) shows coexisting blue and red lines for the interferometer loop but not between source S and beam splitter BS2 (no red probability) nor between beam split-

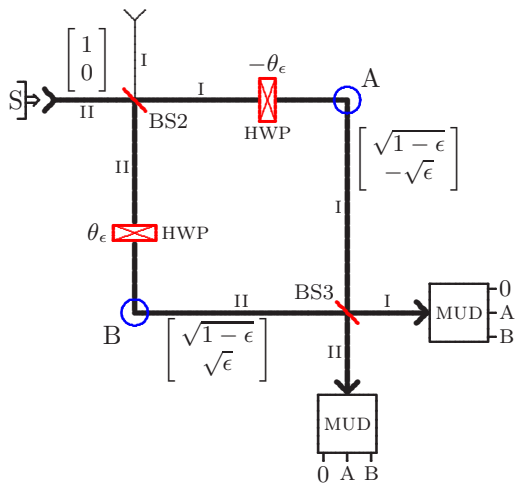


FIG. 8. Single-photon two-path interferometer with the path marked on the polarization. Source S emits one photon at a time, vertically polarized, into the interferometer. The half-wave plates (HWPs) rotate the polarization slightly, such that the amplitude for vertical polarization is $\sqrt{1-\epsilon}$ in both paths, while the horizontal polarization has amplitude $\sqrt{\epsilon}$ for the photons passing through checkpoint A, and amplitude $-\sqrt{\epsilon}$ for those passing through checkpoint B. At each exit port, a measurement for unambiguous discrimination (MUD, see Fig. 11) between the two polarization states is executed when the photon is detected.

ter BS3 and detector D (no blue probability). Shall we, therefore, adopt the narrative that the particle was inside the loop but did not enter or leave? Certainly not. Further, the weak values of the projectors on paths I and II at checkpoints A and B are ill-defined unless there is an interferometer phase with $e^{i\varphi} \neq 1$. Then these weak values are $\frac{1}{2} \pm \frac{1}{2i} \cot \frac{\varphi}{2}$, and Fig. 7(c) applies for $0 \neq \varphi \rightarrow 0$. We do not offer a physical interpretation of these weak values and leave the matter at that [54].

VII. SINGLE-PHOTON TWO-PATH INTERFEROMETER WITH MARKED PATHS AND UNAMBIGUOUS PATH KNOWLEDGE

A. The interfering photon carries the polarization

One experimental realization of the two-path interferometer of Fig. 7 with photons as the interfering particles is sketched in Fig. 8, where we use the photon's polarization degree of freedom as the path-marker qubit. The path-marker amplitudes v and h in $\begin{bmatrix} v \\ h \end{bmatrix}$ now refer to the vertical and horizontal polarization, respectively, and all photons are vertically polarized before entering the interferometer loop at beam splitter BS2.

Inside the interferometer, we have half-wave plates (HWPs) set at angles $-\theta_\epsilon$ in path I and θ_ϵ in path II, with $\cos(2\theta_\epsilon) = \sqrt{1-\epsilon}$ and $\sin(2\theta_\epsilon) = \sqrt{\epsilon}$. The effect of a half-wave plate on the two-component column of polar-

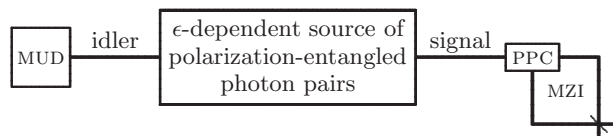


FIG. 9. Scheme of the photon-pair experiment. The source emits an idler-signal pair of polarization-entangled photons in a state determined by the ϵ parameter of Eq. (61). The signal enters the Mach-Zehnder interferometer (MZI) with a polarization-to-path converter (PPC, see Fig. 10) at the entrance. The idler polarization is correlated with the signal path through the MZI. The measurement for unambiguous discrimination (MUD, see Fig. 11) extracts this path information from the idler polarization.

ization amplitudes is described by the two-by-two matrix in

$$\begin{bmatrix} v \\ h \end{bmatrix} \xrightarrow[\text{at } \theta]{\text{HWP}} \begin{bmatrix} \cos(2\theta) & \sin(2\theta) \\ \sin(2\theta) & -\cos(2\theta) \end{bmatrix} \begin{bmatrix} v \\ h \end{bmatrix}. \quad (69)$$

Therefore, we have the columns of Eq. (61) for the polarizations of the photons after the half-wave plates, so that these polarizations are associated with the respective checkpoints. At each exit, the photons are detected by a measurement for unambiguous discrimination (MUD) that has the three outcome operators of Eqs. (64) and (65); its realization is described below (see Fig. 11).

In the verification mode of Fig. 7(b), beam splitter BS3 is removed. Alice knows which measurement for unambiguous discrimination detected the photon, while Bob is told which outcome was found (0 or A or B) but not at which exit.

The single-photon experiment of Fig. 8 correctly implements the scheme of Fig. 7 but it suffers from the drawback that the interfering particle is also the carrier of the path-marker qubit. We cannot detect the particle (\equiv the photon) without at the same time measuring the path-marker qubit (\equiv its polarization). Then, the distinction between observers Alice and Bob is rather artificial: The verification described in the preceding paragraph would require an arbiter who, after noting at which of the six outcomes of both measurements for unambiguous discrimination the photon was registered, informs Alice about the exit and Bob about the outcome.

Therefore, an experimental implementation in which the path qubit and the path-marker qubit are physically separated and can be measured individually is desirable. We describe such an implementation in the next section.

B. A partner photon carries the polarization

The scheme is presented in Fig. 9. The two-photon source is of the kind pioneered by Kwiat *et al.* [55] (see also [56]), in which spontaneous parametric down-conversion produces photon pairs (“signal” and “idler”)

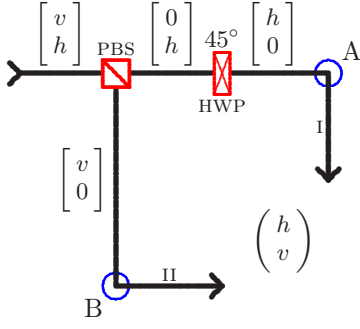


FIG. 10. Conversion of a polarization qubit into a path qubit. The polarizing beam splitter (PBS) reflects vertical polarization and transmits horizontal polarization; the half-wave plate (HWP) at 45° turns the horizontal polarization into vertical polarization. The overall effect is the conversion of the polarization qubit carried by the incoming photon into a path qubit of a vertically polarized photon such that the amplitude for the initial horizontal polarization becomes the amplitude for path I, and the initial vertical-polarization amplitude becomes the path-II amplitude.

in a polarization-entangled state with the wave function

$$\sqrt{1-\epsilon} \begin{bmatrix} 1 \\ 0 \end{bmatrix} \otimes \begin{bmatrix} 1 \\ 0 \end{bmatrix} + \sqrt{\epsilon} \begin{bmatrix} 0 \\ 1 \end{bmatrix} \otimes \begin{bmatrix} 0 \\ 1 \end{bmatrix}, \quad (70)$$

where the first factor in the tensor product is for the idler polarization and the second for the signal polarization. Consistent with the meaning of the two-component columns in Eq. (69) and Fig. 8, the probability for finding both photons vertically polarized is $1-\epsilon$, and that for both horizontally polarized is ϵ . Before leaving the source, the signal traverses a half-wave plate set at 22.5° , which turns the wave function into

$$\begin{aligned} & \sqrt{\frac{1-\epsilon}{2}} \begin{bmatrix} 1 \\ 0 \end{bmatrix} \otimes \begin{bmatrix} 1 \\ 1 \end{bmatrix} + \sqrt{\frac{\epsilon}{2}} \begin{bmatrix} 0 \\ 1 \end{bmatrix} \otimes \begin{bmatrix} 1 \\ -1 \end{bmatrix} \\ &= \frac{1}{\sqrt{2}} \begin{bmatrix} \sqrt{1-\epsilon} \\ \sqrt{\epsilon} \end{bmatrix} \otimes \begin{bmatrix} 1 \\ 0 \end{bmatrix} + \frac{1}{\sqrt{2}} \begin{bmatrix} \sqrt{1-\epsilon} \\ -\sqrt{\epsilon} \end{bmatrix} \otimes \begin{bmatrix} 0 \\ 1 \end{bmatrix}, \quad (71) \end{aligned}$$

where we recognize the wave functions of Eq. (61) in the idler factors. This is the polarization-entangled idler-signal state emitted by the source.

The signal enters the Mach-Zehnder interferometer loop, which has a polarization-to-path converter (PPC) at the entrance. As explained in the caption to Fig. 10, it turns the polarization qubit with the wave function $\begin{bmatrix} v \\ h \end{bmatrix}$ into a path qubit with the wave function $\begin{pmatrix} h \\ v \end{pmatrix}$. Accordingly, the idler-signal pair of photons is then prepared in the state

$$\frac{1}{\sqrt{2}} \begin{bmatrix} \sqrt{1-\epsilon} \\ -\sqrt{\epsilon} \end{bmatrix} \otimes \begin{pmatrix} 1 \\ 0 \end{pmatrix} + \frac{1}{\sqrt{2}} \begin{bmatrix} \sqrt{1-\epsilon} \\ \sqrt{\epsilon} \end{bmatrix} \otimes \begin{pmatrix} 0 \\ 1 \end{pmatrix}, \quad (72)$$

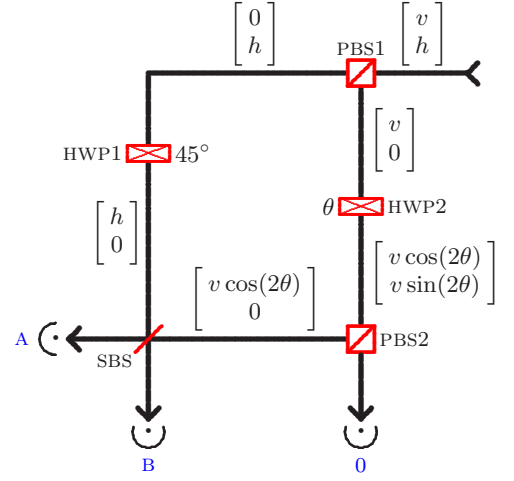


FIG. 11. Unambiguous discrimination of two polarization states. At the entrance, a polarizing beam splitter (PBS1) separates the amplitude h for horizontal polarization from the amplitude v for vertical polarization. The horizontally polarized component is converted to vertical polarization by a half-wave plate at 45° (HWP1) and then reaches the symmetric beam splitter SBS. It is re-united there with the vertical-polarization amplitude v , diminished in strength by the combined effect of HWP2, set at angle θ , and PBS2. The horizontally polarized amplitude $v \sin(2\theta)$ introduced by HWP2 is transmitted by PBS2 and may then trigger a detector (outcome 0). The two other detectors (outcomes A and B) respond to photons at the exit ports of SBS.

which is exactly the situation depicted in Fig. 8 after the photon has passed checkpoints A or B, except that now the polarization is that of the partner photon (idler) rather than the Mach-Zehnder-interfering photon (signal). The further fate of the signal is either as in Fig. 7(a) when the interferometer is closed and we condition on detecting the photon at exit II, or as in Fig. 7(b) when beam splitter BS3 is removed and the photon can be detected at exit I or at exit II. With a suitably long delay line in the signal path from the source to the interferometer, it is possible to postpone Alice's decision between the "wave mode" of Fig. 7(a) and the "particle mode" of Fig. 7(b) until after Bob has measured the idler polarization and announced whether he bets on one of the signal paths or not.

The fate of the idler is different. We examine its polarization with the measurement for unambiguous discrimination (MUD) with the outcome operators of Eq. (64) for the conclusive results and the outcome operator of Eq. (65) for the inconclusive result. This measurement can be implemented by the setup of Fig. 11; see [48] or [57] for similar but different setups.

An idler with initial polarization state $\begin{bmatrix} v \\ h \end{bmatrix}$ is detected by the three detectors with the probabilities

$$p_A = \frac{1}{2} |v \cos(2\theta) - h|^2 \quad \text{for outcome A,}$$

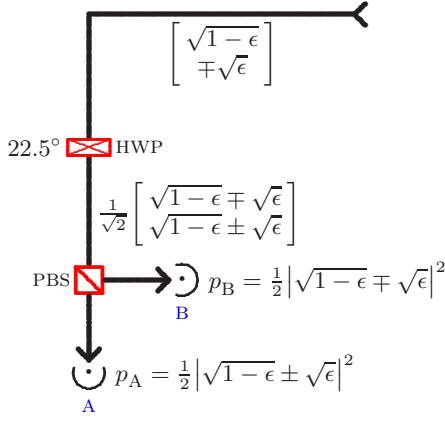


FIG. 12. Measurement for error minimization. The idler passes through the half-wave plate (HWP) at 22.5° and is then sent to one of the two detectors by the polarizing beam splitter (PBS). We bet on signal path I (checkpoint A) if detector A registers the idler, and on path II (checkpoint B) if detector B fires.

$$p_B = \frac{1}{2} |v \cos(2\theta) + h|^2 \quad \text{for outcome B,}$$

$$p_0 = |v \sin(2\theta)|^2 \quad \text{for outcome 0,} \quad (73)$$

where θ is the angle at which the half-wave plate HWP2 in Fig. 11 is set. Both polarization states to be distinguished have $v = \sqrt{1-\epsilon}$, and there is $h = -\sqrt{\epsilon}$ for signal path I (checkpoint A) or $h = \sqrt{\epsilon}$ for signal path II (checkpoint B). Therefore, the choice $\cos(2\theta) = \sqrt{\epsilon/(1-\epsilon)}$ ensures unambiguous discrimination:

$$p_A = \begin{cases} 2\epsilon & \text{for checkpoint A,} \\ 0 & \text{for checkpoint B,} \end{cases}$$

$$p_B = \begin{cases} 0 & \text{for checkpoint A,} \\ 2\epsilon & \text{for checkpoint B,} \end{cases}$$

$$p_0 = 1 - 2\epsilon \quad \text{for both checkpoints.} \quad (74)$$

Prior to performing the experiment of Fig. 9, one should verify that the setup is properly aligned. For this purpose, we vary the phase in the Mach-Zehnder interferometer and record the interference pattern to confirm that the fringe visibility is $1 - 2\epsilon$. We also measure the idler polarization with the error-minimizing measurement [45] of Fig. 12 that maximizes our chance of guessing the path right [58, 59] and so confirm that we guess right for the fraction $\frac{1}{2} + \sqrt{\epsilon(1-\epsilon)}$ of all signals.

The experiment of Fig. 8, in the version of Figs. 9 to 12, has been performed and the results are in full agreement with the theoretical predictions [38]. In particular, the experiment confirms that every signal detected at exit II has a known path through the interferometer irrespective of the value of ϵ .

VIII. SINGLE-PHOTON VERSION OF THE EXPERIMENT BY DANAN *ET AL.* [3]

In the three-path interferometer of Figs. 1, 2, 4, and 6, we have the wave function in Eq. (40) for the entangled state of the interfering particle and the path marker after unitary operators A, B, C acted when the particle passed checkpoints A, B, C and before the path amplitudes are processed by beam splitters BS3 and BS4. That is, Eq. (40) refers to the state of affairs depicted in Fig. 4 before the particle is detected at one of the exit ports or the path marker is measured for unambiguous path discrimination. Now, just as we did in Sec. VII B for the two-path interferometer of Figs. 7–10, we can also here ask: Which pre-entangled initial state Ψ_{ini} for the path marker and the particle would yield Eq. (40) upon the action of $U_2 U_1$ on the particle's path amplitudes? The answer is

$$\begin{aligned} \Psi_{\text{ini}} &= (U_2 U_1)^\dagger \frac{1}{\sqrt{3}} \begin{pmatrix} \psi_A \\ \psi_B \\ \psi_C \end{pmatrix} \\ &= \frac{1}{\sqrt{18}} \begin{pmatrix} -\sqrt{3}(\psi_B - \psi_A) \\ 2\psi_C - \psi_B - \psi_A \\ \sqrt{2}(\psi_C + \psi_B + \psi_A) \end{pmatrix} \\ &= \sqrt{\epsilon} \begin{bmatrix} 1 \\ 0 \\ 0 \end{bmatrix} \otimes \begin{pmatrix} 1 \\ 0 \\ 0 \end{pmatrix} + \sqrt{\epsilon} \begin{bmatrix} 0 \\ 1 \\ 0 \end{bmatrix} \otimes \begin{pmatrix} 0 \\ 1 \\ 0 \end{pmatrix} \\ &\quad + \sqrt{1-2\epsilon} \begin{bmatrix} 0 \\ 0 \\ 1 \end{bmatrix} \otimes \begin{pmatrix} 0 \\ 0 \\ 1 \end{pmatrix}, \quad (75) \end{aligned}$$

as illustrated by Fig. 13.

This observation suggests the following proposal for a single-photon version of the experiment by Danan *et al.* [3], an analog of the signal-idler scheme of Sec. VII B. There, we have the path qubit of the signal entangled with the polarization qubit of the idler; here, the path qubit of the signal is entangled with a path qubit of the idler. The signal traverses Vaidman's three-path interferometer, and the idler is measured either in accordance with Eqs. (30)–(35) for the purpose of unambiguous discrimination of the signal path or in accordance with Eqs. (55)–(57) for the defense of common sense.

The entangled idler-signal state of Eq. (70) uses a single pair of corresponding propagation directions on the cone of down-converted photons emitted by the double-crystal that converts photons from the short-wavelength pump beam into long-wavelength entangled photon pairs [55]. We now use two pairs of corresponding propagation directions and have the idler-signal wave function

$$\frac{1}{\sqrt{2}} \left[\left(\sqrt{\frac{\epsilon}{1-\epsilon}} \begin{bmatrix} 1 \\ 0 \end{bmatrix} \otimes \begin{bmatrix} 1 \\ 0 \end{bmatrix} + \sqrt{\frac{1-2\epsilon}{1-\epsilon}} \begin{bmatrix} 0 \\ 1 \end{bmatrix} \otimes \begin{bmatrix} 0 \\ 1 \end{bmatrix} \right) \otimes \psi_{k_1} \right]$$

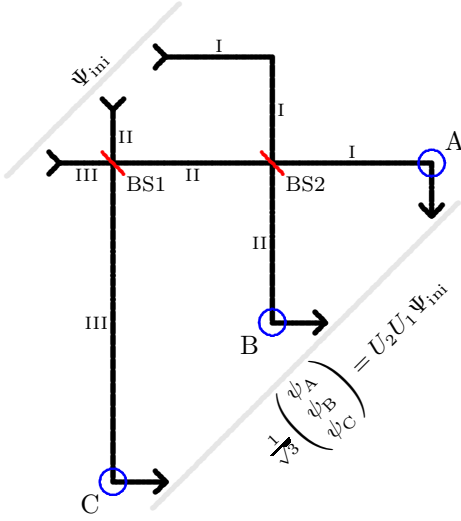


FIG. 13. The preparation stage of Vaidman's interferometer produces an equal-weight superposition of the particle's three paths and entangles the particle with the path marker. The entangled particle–path-marker state of Eq. (40), which describes the situation after the particle has passed checkpoints A, B, or C, can be realized by the action of beam splitters BS1 and BS2 on the pre-entangled state Ψ_{ini} of Eq. (75).

$$+ \left(\sqrt{\frac{\epsilon}{1-\epsilon}} \begin{bmatrix} 1 \\ 0 \end{bmatrix} \otimes \begin{bmatrix} 1 \\ 0 \end{bmatrix} + \sqrt{\frac{1-2\epsilon}{1-\epsilon}} \begin{bmatrix} 0 \\ 1 \end{bmatrix} \otimes \begin{bmatrix} 0 \\ 1 \end{bmatrix} \right) \otimes \psi_{\mathbf{k}_2}, \quad (76)$$

where the tensor products of the two-component columns have the same meaning as in Eq. (70) and the spatial wave functions $\psi_{\mathbf{k}_1}$ and $\psi_{\mathbf{k}_2}$ refer to the respective propagation directions, specified by the signal wave vectors \mathbf{k}_1 and \mathbf{k}_2 . The probability amplitudes of $\sqrt{\epsilon/(1-\epsilon)}$ for the vertical-vertical components and $\sqrt{(1-2\epsilon)/(1-\epsilon)}$ for the horizontal-horizontal components are adjusted by setting the polarization of the pump beam accordingly.

We remove the $\begin{bmatrix} 0 \\ 1 \end{bmatrix} \otimes \begin{bmatrix} 0 \\ 1 \end{bmatrix} \otimes \psi_{\mathbf{k}_1}$ component by a polarizer in the first path of the signal (or in the corresponding idler path) and so reduce the wave function in Eq. (76) to

$$\sqrt{\epsilon} \begin{bmatrix} 1 \\ 0 \end{bmatrix} \otimes \begin{bmatrix} 1 \\ 0 \end{bmatrix} \otimes \psi_{\mathbf{k}_1} + \left(\sqrt{\epsilon} \begin{bmatrix} 1 \\ 0 \end{bmatrix} \otimes \begin{bmatrix} 1 \\ 0 \end{bmatrix} + \sqrt{1-2\epsilon} \begin{bmatrix} 0 \\ 1 \end{bmatrix} \otimes \begin{bmatrix} 0 \\ 1 \end{bmatrix} \right) \otimes \psi_{\mathbf{k}_2}. \quad (77)$$

The $\psi_{\mathbf{k}_1}$ component has the idler and the signal vertically polarized, and the same is the case for the $\psi_{\mathbf{k}_2}$ component after converting the polarization qubits to path qubits as in Fig. 10. We then have the wave function

$$\Psi_{\text{ini}} = \sqrt{\epsilon} \begin{pmatrix} 1 \\ 0 \\ 0 \end{pmatrix} \otimes \begin{pmatrix} 1 \\ 0 \\ 0 \end{pmatrix} + \sqrt{\epsilon} \begin{pmatrix} 0 \\ 1 \\ 0 \end{pmatrix} \otimes \begin{pmatrix} 0 \\ 1 \\ 0 \end{pmatrix}$$

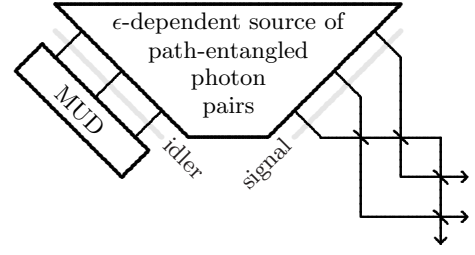


FIG. 14. Scheme of the single-photon version of the experiment by Danan *et al.* [3]. The source prepares idler-signal pairs in the path-entangled state of Eq. (78). The signal traverses Vaidman's three-path interferometer of Fig. 1. The idler enters the apparatus for the measurement for unambiguous discrimination (MUD), by which we gain information about the path taken by the signal.

$$+ \sqrt{1-2\epsilon} \begin{pmatrix} 0 \\ 0 \\ 1 \end{pmatrix} \otimes \begin{pmatrix} 0 \\ 0 \\ 1 \end{pmatrix} \quad (78)$$

for the initial path-entangled idler-signal state where the column entries are path-qutrit probability amplitudes. This Ψ_{ini} has exactly the structure of the Ψ_{ini} in Eq. (75), with the unspecified path-marker qutrit now identified with the path qutrit of the idler.

The source in Fig. 14 prepares the idler-signal pairs in the path-entangled state of Eq. (78). The signal is fed into Vaidman's three-path interferometer, operated with two, three, or all four beam splitters as depicted in Fig. 4, Fig. 6, or Fig. 1, respectively. The idler is measured for unambiguous discrimination of the three signal paths identified in Fig. 4, or for unambiguous discrimination of exits II and III in Fig. 6.

The unambiguous discrimination of the three idler states with the wave functions of Eq. (29) is achieved by the setup of Fig. 15. In a first step, a half-wave plate set at angle θ with $\cos(2\theta) = \sqrt{\epsilon/(1-2\epsilon)}$ converts the path-III amplitude of $\sqrt{1-2\epsilon}$ into amplitude $\sqrt{\epsilon}$ for vertical polarization and amplitude $\sqrt{1-3\epsilon}$ for horizontal polarization. A polarizing beam splitter guides the horizontal component to the “0” detector of the inconclusive outcome which, we recall, indicates path III for signals detected by D when all four beam splitters are in place in Vaidman's interferometer. The overall effect on the remaining probability amplitudes of the path qutrit of the vertically polarized idler is the transition

$$\begin{pmatrix} z_I \\ z_{II} \\ \sqrt{1-2\epsilon} \end{pmatrix} \rightarrow \begin{pmatrix} z_I \\ z_{II} \\ \sqrt{\epsilon} \end{pmatrix} \quad (79)$$

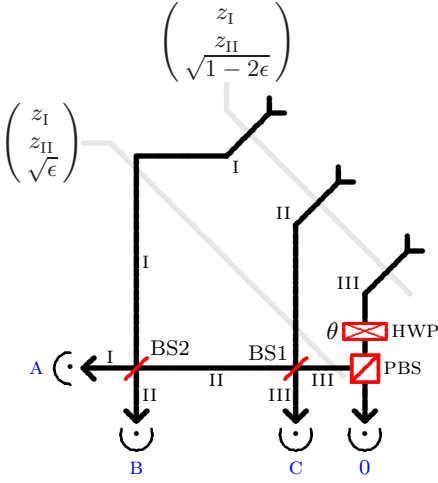


FIG. 15. Unambiguous discrimination of the three states of the idler path qutrit. The arriving idler is vertically polarized. A half-wave plate, in conjunction with a polarizing beam splitter, reduces the path-III amplitude from $\sqrt{1-2\epsilon}$ to $\sqrt{\epsilon}$ before the idler enters a copy of the preparation stage of Vaidman's interferometer. The idler is detected after being processed by beam splitters BS1 and BS2 to yield unambiguous information whether the signal passed checkpoint A, B, or C. The horizontally polarized component introduced by the half-wave plate accounts for the inconclusive outcome.

where

$$\begin{pmatrix} z_I \\ z_{II} \end{pmatrix} = \begin{cases} \begin{pmatrix} \sqrt{3\epsilon/2} \\ -\sqrt{\epsilon/2} \end{pmatrix} & \text{for signal checkpoint A,} \\ \begin{pmatrix} -\sqrt{3\epsilon/2} \\ -\sqrt{\epsilon/2} \end{pmatrix} & \text{for signal checkpoint B,} \\ \begin{pmatrix} 0 \\ \sqrt{2\epsilon} \end{pmatrix} & \text{for signal checkpoint C.} \end{cases} \quad (80)$$

These three columns of idler-path-qutrit amplitudes are pairwise orthogonal and make up a three-by-three matrix that is proportional to $(U_2U_1)^\dagger$,

$$\begin{pmatrix} \sqrt{3\epsilon/2} & -\sqrt{3\epsilon/2} & 0 \\ -\sqrt{\epsilon/2} & -\sqrt{\epsilon/2} & \sqrt{2\epsilon} \\ \sqrt{\epsilon} & \sqrt{\epsilon} & \sqrt{\epsilon} \end{pmatrix} = \sqrt{3\epsilon} (U_2U_1)^\dagger. \quad (81)$$

Therefore, the application of U_2U_1 turns the three

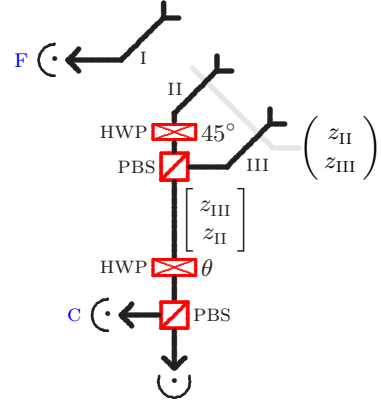


FIG. 16. The orthogonal measurement that distinguishes the idler-path-qutrit states of Eq. (55). Upon detection of the idler at exits “C” or “F”, we know that the signal reached beam splitter BS4 via checkpoints C or F in Fig. 1, respectively, before being detected by detector D. No idler is detected at the third exit.

columns into single-path columns,

$$U_2U_1 \begin{pmatrix} z_I \\ z_{II} \\ \sqrt{\epsilon} \end{pmatrix} = \begin{cases} \begin{pmatrix} \sqrt{3\epsilon} \\ 0 \\ 0 \end{pmatrix} & \text{for signal checkpoint A,} \\ \begin{pmatrix} 0 \\ \sqrt{3\epsilon} \\ 0 \end{pmatrix} & \text{for signal checkpoint B,} \\ \begin{pmatrix} 0 \\ 0 \\ \sqrt{3\epsilon} \end{pmatrix} & \text{for signal checkpoint C,} \end{cases} \quad (82)$$

and this mapping is realized by the preparation-half of Vaidman's interferometer in Fig. 15. Without elaborating on this, we note in passing that the minimum-error measurement is performed by the setup of Fig. 15 with the half-wave plate, the polarizing beam splitter, and detector “0” removed.

The orthogonal measurement that distinguishes the three idler states with the wave functions of Eq. (55) is realized by the setup of Fig. 16. For ϕ_{III} , we simply detect the idler in path I. For ϕ_I and ϕ_{II} , we convert the path qubit of the idler paths II and III with the probability amplitudes z_{II} and z_{III} into a polarization qubit (the reversal of the polarization-to-path conversion in Fig. 10), then rotate the polarization by a half-wave plate set at θ with $\cos(2\theta) = \sqrt{1-2\epsilon}$ and $\sin(2\theta) = \sqrt{2\epsilon}$, and finally use a polarizing beam splitter to separate the resulting vertical and horizontal components.

IX. SUMMARY

Our analysis of Vaidman's three-path interferometer with weak path marking has established that common sense does not mislead us. If there is only one path

available for the particle's journey from the source to the detector, then this path is indeed taken. Such statements about the actual path through the interferometer are meaningful only if they represent path knowledge acquired by a suitable observation. Here, this is achieved by examining the faint traces left by the particle on its way from the source to the detector. Depending on which information we wish to gain, we examine these traces by one measurement or another. In the case of Vaidman's interferometer, we can know for each particle detected by D whether it arrived via the internal loop or not. In the limit of ever fainter traces, all detected particles bypass the loop — exactly as common sense tells us. Vaidman's criterion (5) does not correctly identify the path taken by the particle. These conclusions can be confirmed by a single-particle version of the experiment by Danan *et al.*

[3]; we propose an explicit scheme for that. Finally, we note that others have also concluded, with a variety of arguments, that the common sense reasoning is all right, notably Li *et al.* [4], Sokolovski [22], and Griffiths [23].

ACKNOWLEDGMENTS

BGE is sincerely grateful for insightful discussions with Lev Vaidman, Saverio Pascazio, and Reinhard Werner. We acknowledge Daniel Terno's valuable feedback on an earlier version of the text. This work is funded by the Singapore Ministry of Education (partly through the Academic Research Fund Tier 3 MOE2012-T3-1-009) and the National Research Foundation of Singapore. HKN is also funded by a Yale-NUS College start-up grant.

Appendix: Miscellanea

For reference, we report some technical details here. This could be helpful for a reader who wants to confirm various statements in the text “on the fly.”

The three ways of splitting the overall unitary operator

$$U_4 U_3 U_2 U_1 = \frac{1}{3} \begin{pmatrix} 0 & -\sqrt{3} & \sqrt{6} \\ \sqrt{3} & 2 & \sqrt{2} \\ -\sqrt{6} & \sqrt{2} & 1 \end{pmatrix} \quad (\text{A.1})$$

in the rows of Table I are

$$U_4(U_3 U_2 U_1) = \frac{1}{\sqrt{3}} \begin{pmatrix} \sqrt{3} & 0 & 0 \\ 0 & -1 & \sqrt{2} \\ 0 & \sqrt{2} & 1 \end{pmatrix} \frac{1}{\sqrt{3}} \begin{pmatrix} 0 & -1 & \sqrt{2} \\ -\sqrt{3} & 0 & 0 \\ 0 & \sqrt{2} & 1 \end{pmatrix} \quad (\text{A.2})$$

and

$$(U_4 U_3)(U_2 U_1) = \frac{1}{\sqrt{6}} \begin{pmatrix} \sqrt{3} & \sqrt{3} & 0 \\ 1 & -1 & 2 \\ -\sqrt{2} & \sqrt{2} & \sqrt{2} \end{pmatrix} \frac{1}{\sqrt{6}} \begin{pmatrix} \sqrt{3} & -1 & \sqrt{2} \\ -\sqrt{3} & -1 & \sqrt{2} \\ 0 & 2 & \sqrt{2} \end{pmatrix} \quad (\text{A.3})$$

as well as

$$(U_4 U_3 U_2) U_1 = \frac{1}{\sqrt{3}} \begin{pmatrix} 0 & \sqrt{3} & 0 \\ 1 & 0 & \sqrt{2} \\ -\sqrt{2} & 0 & 1 \end{pmatrix} \frac{1}{\sqrt{3}} \begin{pmatrix} \sqrt{3} & 0 & 0 \\ 0 & -1 & \sqrt{2} \\ 0 & \sqrt{2} & 1 \end{pmatrix}. \quad (\text{A.4})$$

Correspondingly, the overall probability amplitude

$$\begin{pmatrix} 0 \\ 0 \\ 1 \end{pmatrix}^\dagger U_4 U_3 U_2 U_1 \begin{pmatrix} 0 \\ 0 \\ 1 \end{pmatrix} = \frac{1}{3} \quad (\text{A.5})$$

can be calculated by five different inner products,

$$\frac{1}{3} = \begin{pmatrix} 0 \\ 0 \\ 1 \end{pmatrix}^\dagger \frac{1}{3} \begin{pmatrix} \sqrt{6} \\ \sqrt{2} \\ 1 \end{pmatrix} = \frac{1}{\sqrt{3}} \begin{pmatrix} 0 \\ \sqrt{2} \\ 1 \end{pmatrix}^\dagger \frac{1}{\sqrt{3}} \begin{pmatrix} \sqrt{2} \\ 0 \\ 1 \end{pmatrix} = \frac{1}{\sqrt{3}} \begin{pmatrix} -1 \\ 1 \\ 1 \end{pmatrix}^\dagger \frac{1}{\sqrt{3}} \begin{pmatrix} 1 \\ 1 \\ 1 \end{pmatrix} = \frac{1}{\sqrt{3}} \begin{pmatrix} -\sqrt{2} \\ 0 \\ 1 \end{pmatrix}^\dagger \frac{1}{\sqrt{3}} \begin{pmatrix} 0 \\ \sqrt{2} \\ 1 \end{pmatrix}$$

$$= \frac{1}{3} \begin{pmatrix} -\sqrt{6} \\ \sqrt{2} \\ 1 \end{pmatrix}^\dagger \begin{pmatrix} 0 \\ 0 \\ 1 \end{pmatrix}. \quad (\text{A.6})$$

Each of these products stands for a probability amplitude of the form $\langle \text{BWD} | \text{FWD} \rangle$ between a ‘‘forward-in-time ket’’ $|\text{FWD}\rangle$ and a ‘‘backward-in-time’’ bra $\langle \text{BWD} |$. The blue intensities in Fig. 2 are proportional to the squares of the amplitudes in the columns that represent the $|\text{FWD}\rangle$ kets, and likewise for the red intensities and the amplitudes of the rows for the $\langle \text{BWD} |$ bras. The weak values in Table I are the normalized matrix elements

$$\frac{\langle \text{BWD} | X | \text{FWD} \rangle}{\langle \text{BWD} | \text{FWD} \rangle} = 3 \langle \text{BWD} | X | \text{FWD} \rangle \quad \text{with} \quad X \hat{=} \begin{pmatrix} 1 & 0 & 0 \\ 0 & 0 & 0 \\ 0 & 0 & 0 \end{pmatrix} \quad \text{or} \quad \begin{pmatrix} 0 & 0 & 0 \\ 0 & 1 & 0 \\ 0 & 0 & 0 \end{pmatrix} \quad \text{or} \quad \begin{pmatrix} 0 & 0 & 0 \\ 0 & 0 & 0 \\ 0 & 0 & 1 \end{pmatrix} \quad (\text{A.7})$$

for paths I, II, and III, respectively.

With unitary operators A , B , C , E , and F marking the path, the overall unitary operator is

$$U_4 \begin{pmatrix} 1 & 0 & 0 \\ 0 & F & 0 \\ 0 & 0 & 1 \end{pmatrix} U_3 \begin{pmatrix} A & 0 & 0 \\ 0 & B & 0 \\ 0 & 0 & C \end{pmatrix} U_2 \begin{pmatrix} 1 & 0 & 0 \\ 0 & E & 0 \\ 0 & 0 & 1 \end{pmatrix} U_1 = \frac{1}{6} \begin{pmatrix} -3(B-A) & -\sqrt{3}(B+A)E & \sqrt{6}(B+A)E \\ \sqrt{3}F(B+A) & 4C + F(B-A)E & \sqrt{2}[2C - F(B-A)E] \\ -\sqrt{6}F(B+A) & \sqrt{2}[2C - F(B-A)E] & 2[C + F(B-A)E] \end{pmatrix}, \quad (\text{A.8})$$

and the analog of Eq. (A.5),

$$\begin{pmatrix} 0 \\ 0 \\ 1 \end{pmatrix}^\dagger U_4 \begin{pmatrix} 1 & 0 & 0 \\ 0 & F & 0 \\ 0 & 0 & 1 \end{pmatrix} U_3 \begin{pmatrix} A & 0 & 0 \\ 0 & B & 0 \\ 0 & 0 & C \end{pmatrix} U_2 \begin{pmatrix} 1 & 0 & 0 \\ 0 & E & 0 \\ 0 & 0 & 1 \end{pmatrix} U_1 \begin{pmatrix} 0 \\ 0 \\ 1 \end{pmatrix} = \frac{1}{3} [C + F(B-A)E], \quad (\text{A.9})$$

can be calculated by eight different inner products,

$$\begin{aligned} \frac{1}{3} [C + F(B-A)E] &= \begin{pmatrix} 0 \\ 0 \\ 1 \end{pmatrix}^\text{T} \frac{1}{6} \begin{pmatrix} \sqrt{6}(B+A)E \\ \sqrt{2}[2C - F(B-A)E] \\ 2[C + F(B-A)E] \end{pmatrix} = \frac{1}{\sqrt{3}} \begin{pmatrix} 0 \\ \sqrt{2} \\ 1 \end{pmatrix}^\text{T} \frac{1}{\sqrt{6}} \begin{pmatrix} (B+A)E \\ F(B-A)E \\ \sqrt{2}C \end{pmatrix} \\ &= \frac{1}{\sqrt{3}} \begin{pmatrix} 0 \\ \sqrt{2}F \\ 1 \end{pmatrix}^\text{T} \frac{1}{\sqrt{6}} \begin{pmatrix} (B+A)E \\ (B-A)E \\ \sqrt{2}C \end{pmatrix} = \frac{1}{\sqrt{3}} \begin{pmatrix} -F \\ F \\ 1 \end{pmatrix}^\text{T} \frac{1}{\sqrt{3}} \begin{pmatrix} AE \\ BE \\ C \end{pmatrix} \\ &= \frac{1}{\sqrt{3}} \begin{pmatrix} -FA \\ FB \\ C \end{pmatrix}^\text{T} \frac{1}{\sqrt{3}} \begin{pmatrix} E \\ E \\ 1 \end{pmatrix} = \frac{1}{\sqrt{6}} \begin{pmatrix} -F(B+A) \\ F(B-A) \\ \sqrt{2}C \end{pmatrix}^\text{T} \frac{1}{\sqrt{3}} \begin{pmatrix} 0 \\ \sqrt{2}E \\ 1 \end{pmatrix} \\ &= \frac{1}{\sqrt{6}} \begin{pmatrix} -F(B+A) \\ F(B-A)E \\ \sqrt{2}C \end{pmatrix}^\text{T} \frac{1}{\sqrt{3}} \begin{pmatrix} 0 \\ \sqrt{2} \\ 1 \end{pmatrix} = \frac{1}{6} \begin{pmatrix} -\sqrt{6}F(B+A) \\ \sqrt{2}[2C - F(B-A)E] \\ 2[C + F(B-A)E] \end{pmatrix}^\text{T} \begin{pmatrix} 0 \\ 0 \\ 1 \end{pmatrix}, \quad (\text{A.10}) \end{aligned}$$

which one could again read as bra-ket products of the $\langle \text{BWD} | \text{FWD} \rangle$ kind only that now the various column entries are operators acting on the degrees of freedom used for the path marking, whereas the column entries in Eq. (A.6) are probability amplitudes for the three paths.

[1] L. Vaidman, Phys. Rev. A **87**, 052104 (2013).

[2] L. Vaidman, Phys. Rev. A **89**, 024102 (2014).

[3] A. Danan, D. Farfurnik, S. Bar-Ad, and L. Vaidman,

Phys. Rev. Lett. **111**, 240402 (2013).

[4] Z.-H. Li, M. Al-Amri, and Z. Zubairy, Phys. Rev. A **88**, 046102 (2013).

- [5] L. Vaidman, Phys. Rev. A **88**, 046103 (2013).
- [6] P. L. Saldanha, Phys. Rev. A **89**, 033825 (2014).
- [7] H. Salih, Front. Phys. **3**, 47 (2015).
- [8] A. Danan, D. Farfurnik, S. Bar-Ad, and L. Vaidman, Front. Phys. **3**, 48 (2015).
- [9] B. E. Y. Svensson, e-print arXiv:1402.4315 [quant-ph] (2014).
- [10] J.-H. Huang, L.-Y. Hu, X.-X. Xu, C.-J. Liu, Q. Guo, H.-L. Zhang, and S.-Y. Zhu, e-print arXiv:1402.4581 [quant-ph] (2014); see also Sec. 3 in [14].
- [11] M. Wieśniak, e-print arXiv:1407.1739 [quant-ph] (2014).
- [12] B. E. Y. Svensson, e-print arXiv:1407.4613 [quant-ph] (2014).
- [13] K. Bartkiewicz, A. Černoč, D. Javůrek, K. Lemr, J. Soubusta, and J. Svolík, Phys. Rev. A **91**, 012103 (2015).
- [14] Z.-Q. Wu, H. Cao, J.-H. Huang, L.-Y. Hu, X.-X. Xu, H.-L. Zhang, and S.Y. Zhu, Opt. Express **23**, 10032 (2015).
- [15] M. A. Alonso and A. N. Jordan, Quantum Stud.: Math. Found. **2**, 255 (2015).
- [16] V. Potoček and G. Ferenczi, Phys. Rev. A **92**, 023829 (2015).
- [17] F. Li, F. A. Hashmi, J. X. Zhang, and J.-Y. Zhu, Chin. Phys. Lett. **32**, 050303 (2015).
- [18] L. Vaidman, Phys. Rev. A **93**, 017801 (2016).
- [19] L. Vaidman, Phys. Rev. A **93**, 036103 (2016).
- [20] K. Bartkiewicz, A. Černoč, D. Javůrek, K. Lemr, J. Soubusta, and J. Svolík, Phys. Rev. A **93**, 036104 (2016).
- [21] F. A. Hashmi, F. Li, S.-Y. Zhu, and M. S. Zubairy, J. Phys. A: Math. Theor. **49**, 345302 (2016).
- [22] D. Sokolovski, Phys. Lett. **A381**, 227 (2017).
- [23] R. B. Griffiths, Phys. Rev. A **94**, 032115 (2016).
- [24] L. Vaidman, e-print arXiv:1610.04781 [quant-ph] (2016).
- [25] L. Vaidman, Phys. Rev. A **95**, 066101 (2017).
- [26] M. Bula, K. Bartkiewicz, A. Černoč, D. Javůrek, K. Lemr, V. Michálek, and J. Soubusta, Phys. Rev. A **94**, 052106 (2016).
- [27] A. Ben-Israel, L. Knips, J. Dziewior, J. Meinecke, A. Danan, H. Weinfurter, and L. Vaidman, Chin. Phys. Lett. **34**, 020301 (2017).
- [28] A. Roy and S. Ghosh, e-print arXiv:1701.03074 [quant-ph] (2017).
- [29] G. N. Nikolaev, JETP Lett. **105**, 152 (2017).
- [30] L. Vaidman, JETP Lett. **105**, 473 (2017).
- [31] L. Vaidman, e-print arXiv:1703.03615 [quant-ph] (2017).
- [32] Z.-Q. Zhou, X. Liu, Y. Kedem, J.-M. Cui, Z.-F. Li, Y.-L. Hua, C.-F. Li, and G.-C. Guo, Phys. Rev. A **95**, 042121 (2017).
- [33] G. N. Nikolaev, JETP Lett. **105**, 475 (2017).
- [34] R. B. Griffiths, Phys. Rev. A **95**, 066102 (2017).
- [35] D. Sokolovski, e-print arXiv:1704.02172 (2017).
- [36] Y. Aharonov, P. G. Bergmann, and J. L. Lebowitz, Phys. Rev. **134**, B1410 (1964).
- [37] Y. Aharonov and L. Vaidman, Phys. Rev. A **41**, 11 (1990).
- [38] Y. L. Len, J. Dai, B.-G. Englert, and L. Krivitsky, e-print arXiv:1708.01408 [quant-ph] (2017).
- [39] While these particular matrices will serve the purpose, more general ones can be considered; see, for example, K. Horia, *Post-selected data in quantum measurements*, B. Sc. thesis, National University of Singapore, 2014.
- [40] Or is it minus-one particle at checkpoint A and plus-one particle each at checkpoints B and C? See Sec. 16.5 in [60].
- [41] Actually, the power spectrum reported in Ref. [3], the squared Fourier transform of an intensity difference, is quadratic in the light intensity and, therefore, outside the scope of linear optics.
- [42] In this respect, the situation is markedly better in the experiment of Zhou *et al.* [32], where electro-optic phase modulators at the checkpoints imprint sidebands of several GHz. A tunable frequency filter selects a narrow frequency range before the photons are detected by detector D, eventually recording the full spectrum of the emerging photons.
- [43] This makes the analysis simpler and more transparent but is not absolutely necessary. What really matters is that the three unitary operators F_{AE} , F_{BE} , and C affect the marker state differently. Eventually, the extraction of path information relies on Eqs. (25) and (28) and it is not important how they come about. In assuming independent and uncorrelated degrees of freedom, we follow the example of Refs. [1–3] and many of the papers in the list of Refs. [4] through [35]. Different authors, however, use different conventions. For instance, Griffiths [23] associates one two-state system (qubit) with each checkpoint. We do not rely on such a specific choice in Secs. III, IV, and V, and the path qutrit of the idler in Sec. VIII is not of this kind either.
- [44] The same destructive interference suppresses the sidebands associated with checkpoints E and F in the experiment of Zhou *et al.* [32].
- [45] C. W. Helstrom, *Quantum Detection and Estimation Theory* (Academic Press, New York, 1976).
- [46] A. Chefles and S. M. Barnett, Phys. Lett. **A250**, 223 (1998).
- [47] A. Peres and D. R. Terno, J. Phys. A: Math. Gen. **31**, 7105 (1998).
- [48] R. B. M. Clarke, A. Chefles, S. M. Barnett, and E. Riis, Phys. Rev. A **63**, 040305 (2001).
- [49] J. A. Bergou, U. Herzog, and M. Hillery, Lect. Notes Phys. **649**, 417 (2004).
- [50] B.-G. Englert and J. Řeháček, J. Mod. Opt. **57**, 218 (2010).
- [51] If Bob has no clue, he says “I cannot infer the path.” Since a particle is never found in more than one place, he does not say “The particle followed all three paths simultaneously.”
- [52] In the jargon of a different context, Bob’s sorting of Alice’s particles into subensembles constitutes “probabilistic remote state preparation.”
- [53] This conclusion is supported by the data reported by Zhou *et al.* [32] in their Figs. 1(b) and 1(c): When the path through checkpoint C is blocked, not only the sideband for C is suppressed but also the carrier frequency that corresponds to the inconclusive outcome of the unambiguous path discrimination.
- [54] See Sec. 17.5 in [60].
- [55] P. G. Kwiat, E. Waks, A. G. White, I. Appelbaum, and P. H. Eberhard, Phys. Rev. A **60**, R773 (1999).
- [56] J. Dai, Y. L. Len, Y. S. Teo, L. A. Krivitsky, and B.-G. Englert, New J. Phys. **15**, 063011 (2013).
- [57] L. Neves, G. Lima, J. Aguirre, F. A. Torres-Ruiz, C. Saavedra, and A. Delgado, New. J. Phys. **11**, 073035 (2009).
- [58] G. Jaeger, A. Shimony, and L. Vaidman, Phys. Rev. A **51**, 54 (1995).
- [59] B.-G. Englert, Phys. Rev. Lett. **77**, 2154 (1996).
- [60] Y. Aharonov and D. Rohrlich, *Quantum Paradoxes — Quantum Theory for the Perplexed* (Wiley-VCH, Weinheim, 2005).